Supporting Information for

Efficient Nitrogen Reduction to Ammonia by Fluorine Vacancies with Multi-step Promoting Effect

Zuochao Wang,[#,a] Xueke Wu,[#,a] Yingnan Qin,[#,a] Yi Han,[a] Dan Zhang,[b] Huan Zhao,[a] Jingqi Chi,[c] Guangrui Xu,[d] Minghui Wang,[a] Shaoxiang Li,[b] Dan Wang,[a] Jianping Lai,[,a] and Lei Wang*[,a,b]*

[a] Key Laboratory of Eco-chemical Engineering, Key Laboratory of Optic-electric Sensing and Analytical Chemistry of Life Science, Taishan Scholar Advantage and Characteristic Discipline Team of Eco Chemical Process and Technology, College of Chemistry and Molecular Engineering, Qingdao University of Science and Technology, Qingdao 266042, P. R. China

[b] Shandong Engineering Research Center for Marine Environment Corrosion and Safety Protection,College of Environment and Safety Engineering, Qingdao University of Science and Technology, Qingdao 266042, P. R. China

[c] College of Chemical Engineering, Qingdao University of Science and Technology, Qingdao 266042, P. R. China

[d] School of Materials Science and Engineering, Qingdao University of Science and Technology, Qingdao 266042, P. R. China.

[#]Equal Contribution

Chemicals: Lanthanum acetate hydrate ($C_6H_9O_6La{\cdot}xH_2O$, Shanghai Aladdin Biochemical Technology Co., Ltd., China, 99.9%). Sodium borohydride ($NaBH_4$, Shanghai Aladdin Biochemical Technology Co., Ltd., China, 98%). Sodium citrate dihydrate ($C_6H_5Na_3O_7{\cdot}2H_2O$, Shanghai Aladdin Biochemical Technology Co., Ltd., China, 99%). Sodium Fluoride (NaF, Kermel (Tianjin) Trading Co., Ltd. China, 98%). Ammonium chloride ($^{14}NH_4Cl$, Tianjin Bodi Chemical Co., Ltd. China, 99.5%; $^{15}NH_4Cl$, Morai Chemical, 99 atom%). Lithium sulfate monohydrate ($Li_2SO_4{\cdot}H_2O$, 99%)

were purchased from Aladdin. Nafion solution (5%) was purchase from Sigma-Aldrich. Ethanol (C_2H_6O) were purchased from Sinopharm Chemical Reagent Co., Ltd. Ultrapure water (Millipore Milli-Q grade) with a resistivity of 18.2 MΩ was used in all the experiments.

Preparation of LaF_3-x NSs. Firstly, 0.632 g of lanthanum acetate and 0.588 g sodium citrate dissolved in 10 mL water and 20 mL water, respectively. Then the two solutions were mixed under the constantly stirring at the room temperature. After 30 mins, 1.05 g sodium fluoride dissolved in 30 mL water and then added into the above solution. Lastly the mixture was transfered into a 100 mL Teflon-lined autoclave and maintained at 180 ℃ for 24 h. After the autoclave cooled down naturally, the products were washed by water and ethanol for 3 times, and received powders LaF_3 nanosheets were dried at 60 ℃ overnight.

Preparation of Fv-LaF_3-x NSs. 20 mg of LaF_3 NSs were added into 20 mL water containing the 0.2 g of sodium borohydride solution and stirring for different time in 0, 1, 2, 3 and 4 h (note as Fv-LaF_3-x nanosheets, x represent for different time).

Characterization. X-ray diffraction (XRD) analysis at a scanning rate of $5\,°\,min^{-1}$ in the 2θ ranges from 20 to 80 ° was used to examine the composition of the as-synthesized samples on X'Pert PRO MPD. Scanning electron microscopy (SEM) measurement was collected on Hitachi, S-8200 to investigate the structure and morphology of the samples. Transmission electron microscopy (TEM) and high-resolution TEM (HRTEM) measurements were performed on JEM-2100UHR with operating at 200 kV. X-ray photoelectron spectrum (XPS) was conducted using a VG ESCALABMK II spectrometer with AlKa (1486.6 eV) photon source. All the electrochemical performances of the

as-synthesized samples were carried out on an electrochemical station (CHI 760E). The 1H NMR spectrum was obtained on a Bruker 500 with Probe TXI at room temperature of 25 ℃ using 3 mm tube. The electrolyte after electrolysis was collected, lyophilized and further dissolved in 1 M HCl solution (D_2O/H_2O mixed solution). The IC data were collected by an IC (863 Basic IC Plus. Metrohm, Switzerland) equipped with a Metrosep C Supp 4-250/4.0 column. N_2-TPD of N_2 experiments were conducted on a Quantachrome ChemBET Pulsar TPR/TPD. These four samples were first pretreated at 150 ℃ for 1 h in a 50 mL/min He stream and then cooled to 50 ℃ under a He atmosphere. These samples were adsorbed to N_2 for 3 h, and the remaining N_2 was purged by He for half an hour. Finally, the desorption of N_2 was carried out by heating from 50 ℃ to 500 ℃ at a rate of 10 ℃ min^{-1}.

Electrochemical measurements. Electrochemical measurements were conducted on a CHI760 Electrochemical Workstation (Shanghai Chenhua Instrument Corporation, China) in a conventional three-electrode cell by using a graphite rod electrode as the counter electrode and a saturated calomel electrode as the reference electrode. For the NRR test, the chronoamperometry experiments were conducted in N_2-saturated 0.1 M Li_2SO_4 solution (Notably, the Li_2SO_4 used was pretreated at 800 ℃ about 4 h in Ar.) with stirring at 450 rpm. Firstly, 5.0 mg of Fv-LaF_3-2 nanosheets were dispersed in Nafion alcohol solution containing 0.5 mL ethanol, 0.5 mL H_2O and 50 μL Nafion (5 wt%). Until sonicated for 1 h, it formed a uniform solution. The carbon-paper electrode was prepared by dropping the obtained solution onto a piece of carbon paper (1×1 cm^2), then 30 μL of the catalyst was dropped onto the carbon cloth surface for further electrochemical tests. All the potentials reported in this work were converted to the reversible hydrogen electrode (RHE). The polarization

curves were obtained at a scan rate of 5 mV s^{-1} in 0.1 M Li_2SO_4 solution. The two electrolytic cells were connected by a salt bridge. The double-cell electrolytic cell consists of two single-cell electrolytic cells made of glass and is equipped with a sealable lid. The lid was drilled by a tool of a specific size and matched with the size of the three electrodes, and the electrolytic cells are connected by a salt bridge. The salt bridge is composed of agar, potassium chloride and ultrapure water. All potentials in the text are based on the reversible hydrogen electrode (RHE).The potentials were converted to the RHE scale according to the following equation:

$$E(RHE) = E(SCE) + (0.244 + 0.059 \times pH)\ V.$$

Before the electrolysis, the electrolyte was presaturated by N_2 gas bubbling for at least 30 min (~50 sccm). The purity grade of the gas used in this work is 99.999%. During the electrolysis, N_2 or Ar (~20 sccm) were continuously bubbled to the electrolyte with stirring. The given potentials were iR compensated (95 %). The temperature was kept at around 25 ℃. Calculation of the Faradaic efficiency and the yield rate.

The yield rate of NH_3 can be calculated as follows:

$$\text{Yield rate} = (c(NH_4^+) \times V)/(m_{cat} \times t)$$

Where $c(NH_4^+)$ is the measured NH_3 concentration, V is the volume of the electrolyte, mcat. is the metal mass of the catalyst (typically 0.15 mg) and t is the reduction time.

The NH_3 yield was calculated using the following equation:

$$\text{Yield rate} = (c(NH_4^+) \times V)/(t \times A)$$

where F is the faraday constant, $c(NH_4^+)$ is the measured concentration of NH_4^+, V is the electrolyte volume, A is the geometric area of the cathode (1 cm^2) and t is the reduction time.

The Faradaic efficiency was estimated from the charge consumed for NH_3 production and the total charge passed through the electrode:

$$\text{Faradaic efficiency} = 3 \times F \times c(NH_4^+) \times V/(17 \times Q)$$

F is the Faraday constant (96 485 C mol^{-1}), Q is the quantity of applied electricity.

The reported NH_3 yield rate, Faradaic efficiency, and error bars were determined by three measurements of independent samples under the same conditions.

Determination of ammonia:

The produced NH_3 was quantitatively determined using the indophenol blue method.[1] Typically, 1 mL of the sample solution was first pipetted from the post-electrolysis electrolyte. Afterward, 1 mL of 1 M NaOH solution containing salicylic acid (5 wt%) and sodium citrate (5 wt%) was added, and 0.5 mL of NaClO solution (0.05 M) and 0.1 mL of sodium nitroferricyanide solution (1 wt%) were added subsequently. After 2 h, the absorption spectra of the resulting solution were acquired with an ultraviolet-visible (UV-vis) spectrophotometer (BioTek Synergy H1 Hybrid Multi-Mode Reader). The formed indophenol blue was measured by absorbance at λ = 655 nm. In specific, 1 mL postelectrolyzed electrolyte was filtered by a nylon membrane filter (220 nm) and then injected directly into the ion chronograph. The NH_4^+ calibration curves were established by a set of standard solutions with different lithium sulfate concentrations. The signal of NH_4^+ in ion chronograph spectra was located at 9.5 min. The concentration (NH_4^+) absorbance curve used for estimation of NH_3 amount was calibrated using standard NH_4Cl solution with NH_4^+ concentrations of 0.0, 0.2, 0.4, 0.6, 0.8, and 1.0 μg mL^{-1} in 0.1 M Li_2SO_4. The fitting curve ($y = 0.509x + 0.04065$, $R^2 = 0.999$) showed

a good linear relation between the NH_4^+ concentration and absorbance.

$^{15}N_2$ isotope labelling experiments. The produced NH_3 was detected by the 1H NMR. $^{15}N_2$ (99%, provided by the Shanghai Aladdin Biochemical Technology Co., Ltd) was used to further verify the N-source of NH_3 produced. All the gases were purified by the Cu impurity trap. Before the electrolysis, the Ar was plunged into the electrolyte about 1 h, then $^{15}N_2$ was plunged into the electrolyte to saturation. The electrolyte after electrolysis at -0.1 V *vs*. RHE was collected, lyophilized, and further dissolved in the solution of 1 M HCl, D_2O and H_2O. Then the $^{15}NH_3$ produced was detected by the ^{1}H NMR spectrum (Bruker 500). The procedure that detected $^{14}NH_3$ produced was the same except the $^{14}N_2$ (99.999%) was used. The standard curves were calibrated by using a series of concentrations of NH_4Cl. And the fitting curves are y=0.034x+0.004, R^2=0.999 and y=0.036x-0.002, R^2=0.998.

Determination of NO_x: NO_x was determined using N-(-1-naphthyl) ethylenediamine dihydrochloride spectrophotometric method with some modification.[2] Specifically, 0.4 g of sulfanilic acid was dissolved in 5 mL of H_2O and 1 mL of phosphoric acid. Then add 20 mg of n-(1-naphthyl)-ethylenediamine dihydrochloride and dilute the volume to 100 mL to obtain the chromogenic agent. 1 mL treated electrolyte was mixed with 4 mL chromogenic agent and left in darkness for 30 min, and measure the UV-Vis absorption spectrum at 540 nm. Calibrate the concentration-absorbance curve with a series of standard potassium nitrite solutions in 0.1 M Li_2SO_4 solution.

In situ surface-enhanced infrared absorption spectroscopy with the attenuated total reflection (ATR-SEIRAS) technique: Silicon planar gold plating film operation process: Preparation of gold plating solution. preparation of solution A：0.1222 g NaOH and 0.2286 g $NaAuCl_4$•$2H_2O$ were dissolve in 3mL deionized water and ultrasound for 1 h. Preparation of solution B：0.134 g NH_4Cl, 0.9468 g Na_2SO_3, and 0.6202 g $Na_2S_2O_3$•$5H_2O$ were all dissolved in 50mL deionized water and

dispersed by ultrasound for 1h. Mixed solution A and solution B, added 50 mL deionized water, and fully ultrasonic for 2 h. Silicon crystal plating preparation：First, soaked the silicon crystal in aqua regia (V_{HCl}: V_{HNO_3}=3: 1) for 30 min, then, rinsed with deionized water. Second, grinded silicon crystal plating on the electrode cloth with 50 μm Al_2O_3 powder clockwise for 10min, and then cleaned with deionized water. Third, treated with deionized water and acetone alternately for 5 times: 2 min, 1 min, 1 min, 1 min, 2 min, respectively. Forth, use oxidizing liquid ($V_{H_2SO_4}$: $V_{H_2O_2}$ = 3:1), took out and rinsed with deionized water. Last, soaked silicon crystal plating in 40% NH_4F solution for 4-5 min, washed with deionized water. Deposition of gold film：First, put 15 mL gold plating solution into a 25 mL beaker, dropped 3.4 mL 2% HF into solution after preheated for 2 min in water bath at 50-55 ℃. Second, immersed the prepared silicon crystal in the above solution for 4-5 min. Finally, the gold plating layer can be obtained by washing with deionized water. All ATR-SEIRAS spectra were carried out in transmission units by subtracting the reference spectrum obtained at -0.1 *vs*. RHE.

Hydrazine quantification. The hydrazine present in the electrolyte was estimated by the method of Watt and Chrisp.[3] First, the preparation of the color developing reagent was carried out by mixing $C_9H_{11}NO$ (5.99 g), HCl (30 mL) and C_2H_5OH (300 mL). Then, 1.0 mL of the electrolyte solution was mixed with 1.0 mL of the color developing reagent, and rapidly stirred at room temperature for 15 min. Finally, the absorbance was measured at a wavelength of 455 nm using a UV-vis 2700 spectrophotometer. The standard curve method was also used to estimate the concentration of N_2H_4 produced in the electrolyte. A fitted curve of 0.1 M Li_2SO_4 solution ($y = 1.184x+0.02371$, R^2=0.999) with N_2H_4 concentrations of 0.0, 0.2, 0.4, 0.6, 0.8 and 1.0 μg mL^{-1} showed a good linear relationship between N_2H_4 concentration and absorbance.

Calculation Setup

DFT calculations were performed in the Vienna ab initio simulation package (VASP). A

spin-polarized GGA PBE functional, all-electron plane-wave basis sets with an energy cutoff of 520 eV, and a projector augmented wave (PAW) method were adopted. A (3×3×1) Monkhorst-Pack mesh was used for the Brillouin-zone integrations to be sampled. The conjugate gradient algorithm was used in the optimization. The convergence threshold was set $1*10^{-4}$ eV in total energy and 0.05 eV/Å in force on each atom.

The adsorption energy change (ΔE_{abs}) was determined as follows:

$$\Delta E_{abs} = E_{total} - E_{sur} - E_{mol}$$

where E_{total} is the total energy for the adsorption state, E_{sur} is the energy of pure surface, E_{mol} is the energy of molecule.

The free energy change (ΔG) for adsorptions were determined as follows:

$$\Delta G = E_{total} - E_{sur} - E_{mol} + \Delta E_{ZPE} - T\Delta S$$

where E_{total} is the total energy for the adsorption state, E_{sur} is the energy of pure surface, ΔE_{ZPE} is the zero-point energy change and ΔS is the entropy change.

Figures

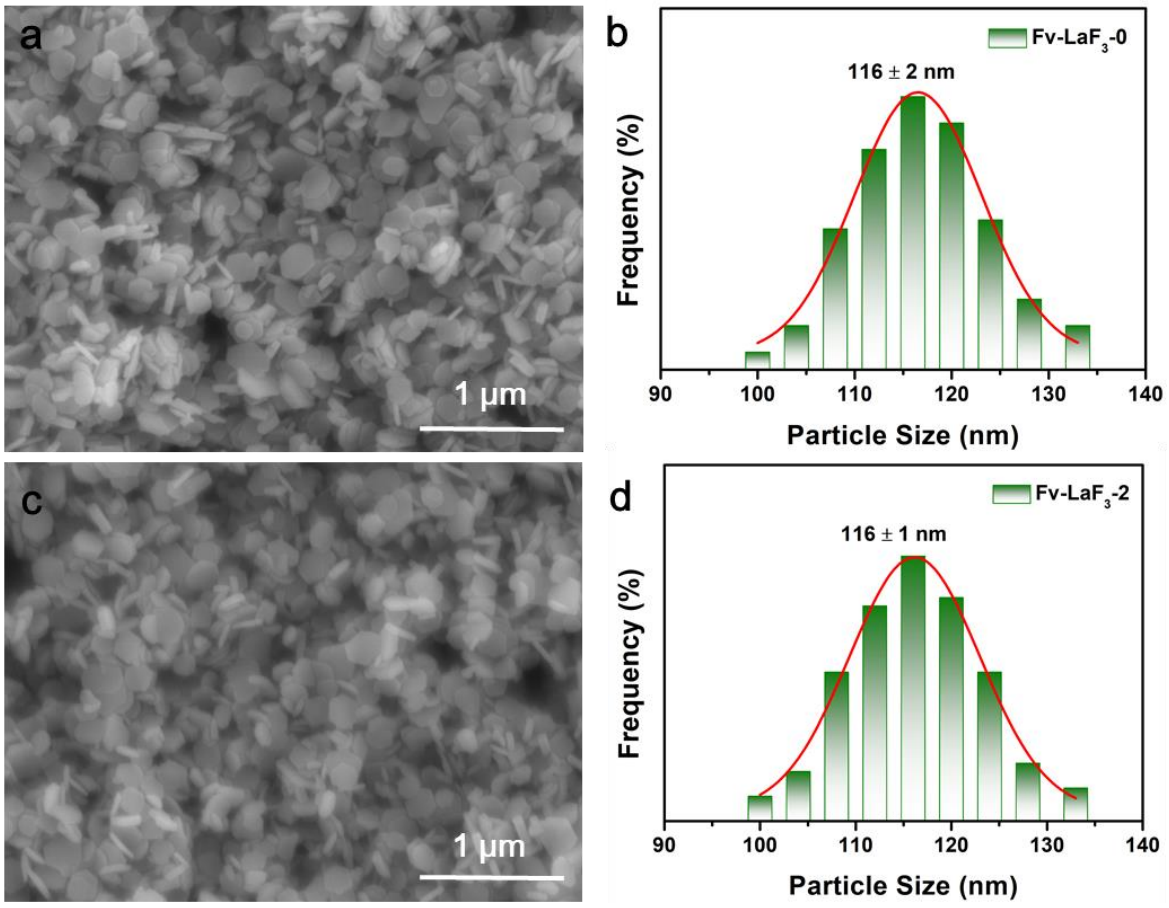

Figure S1. SEM images and particle size histogram for Fv-LaF_3-0 NSs and Fv-LaF_3-2 NSs.

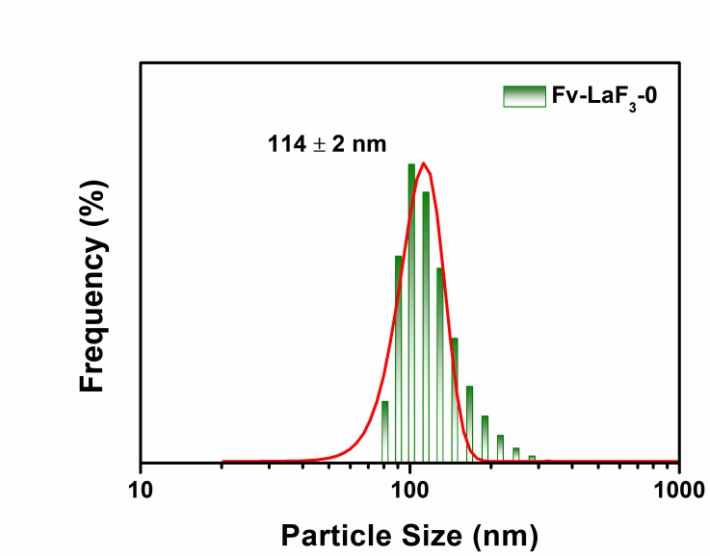

Figure S2. The DLS image of Fv-LaF_3-0 NSs.

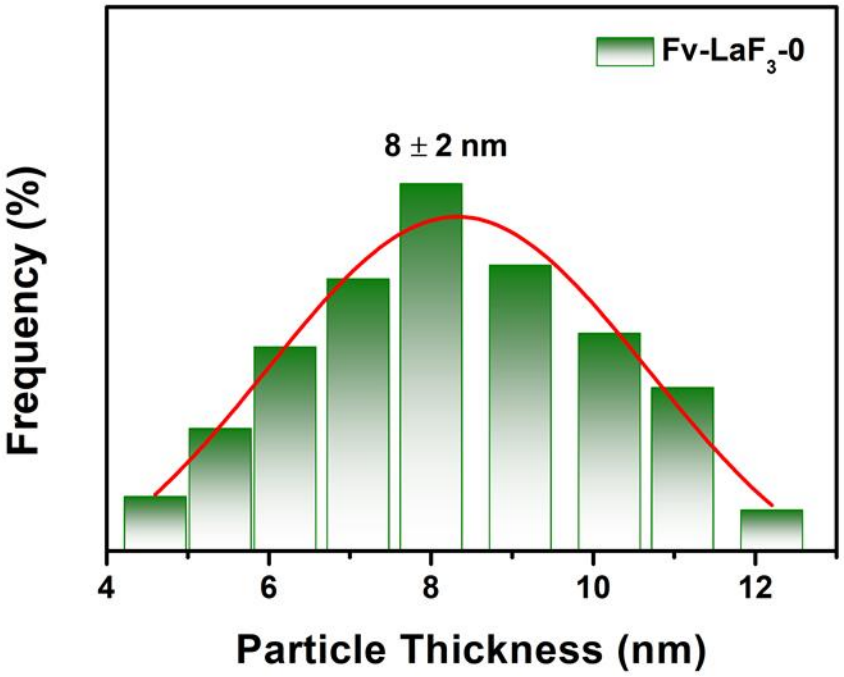

Figure S3. Particle thickness histogram of Fv-LaF_3-0 NSs.

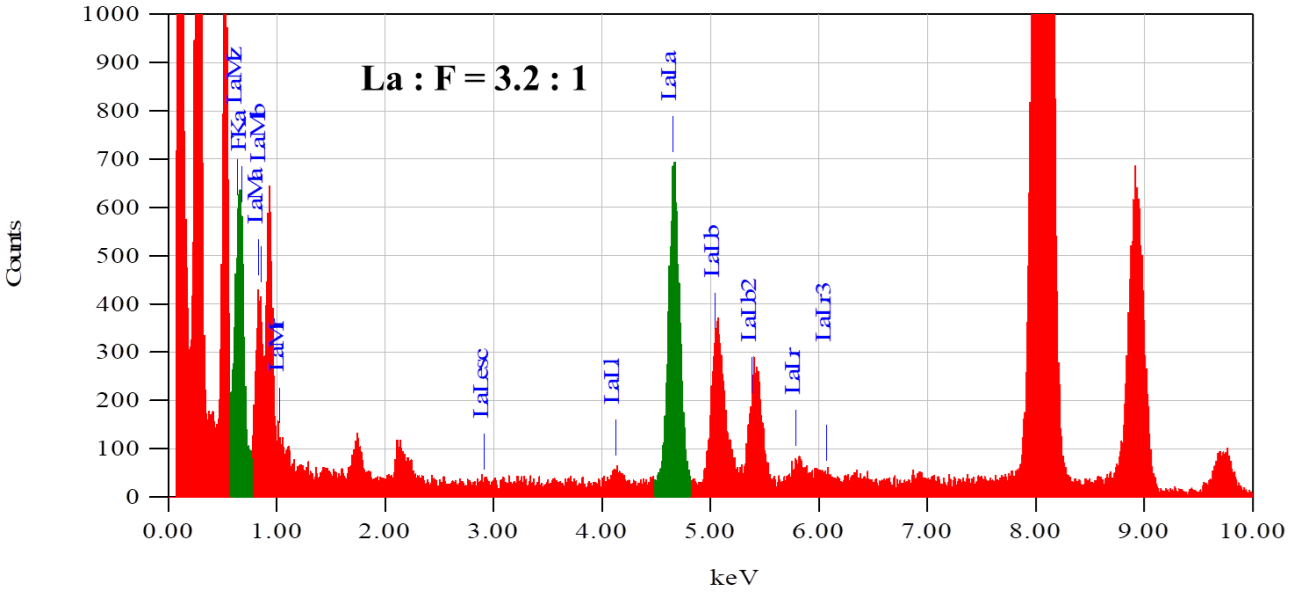

Figure S4. EDX pattern of Fv-LaF_3-2 NSs.

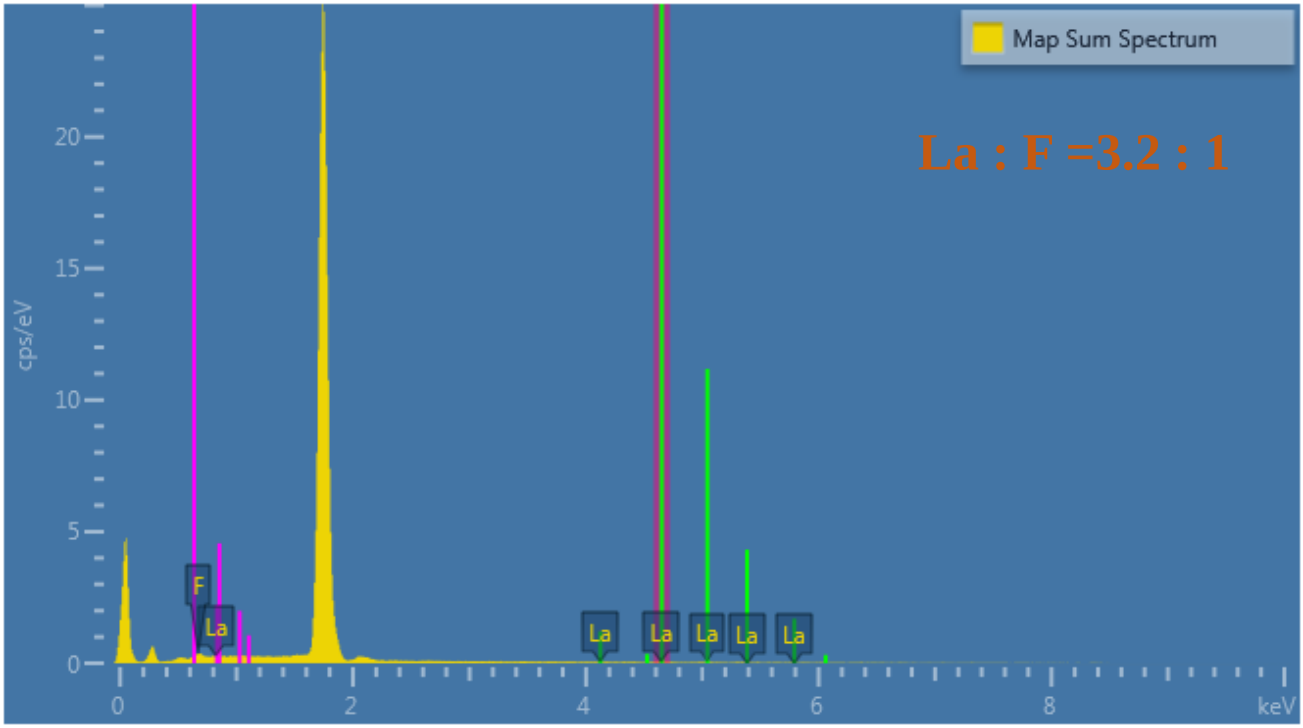

Figure S5. SEM EDX pattern of Fv-LaF_3-2 NSs.

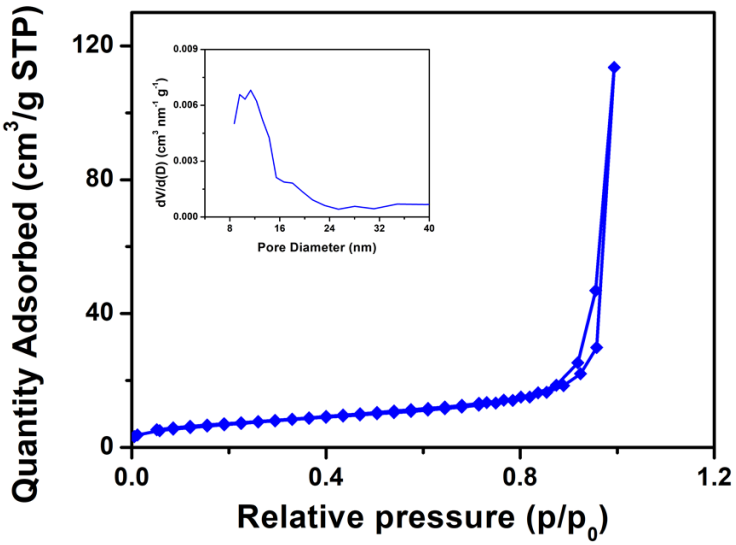

Figure S6. N_2 adsorption and desorption isotherm of Fv-LaF_3-2 NSs (Insets: the corresponding pore distribution).

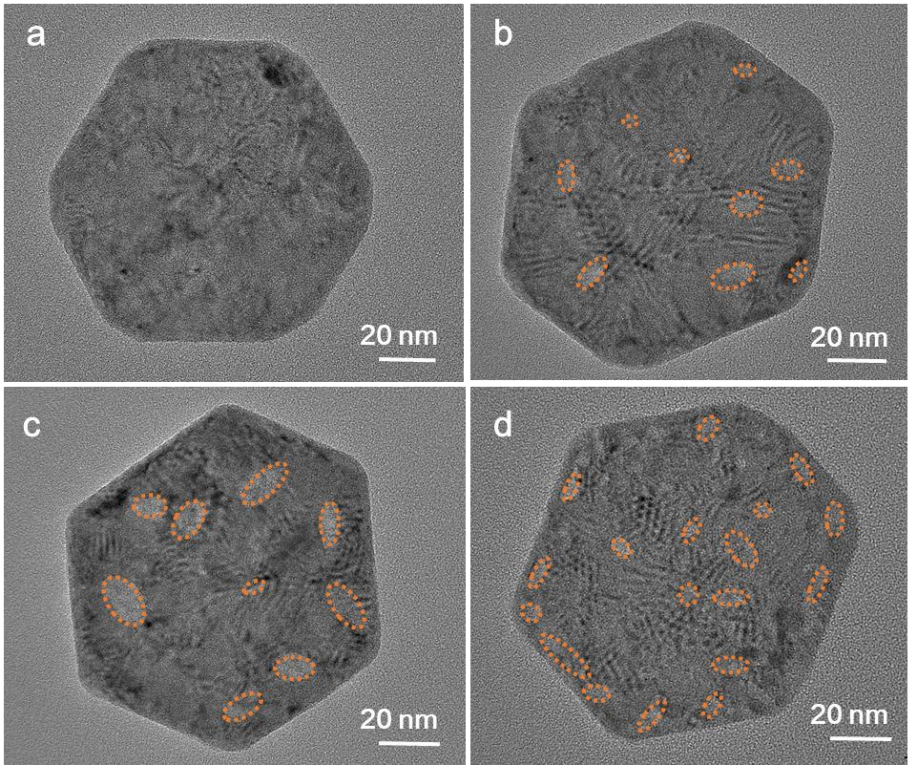

Figure S7. TEM images of (a) Fv-LaF_3-0 NSs, (b) Fv-LaF_3-1 NSs, (c) Fv-LaF_3-2 NSs and (d) Fv-LaF_3-3 NSs.

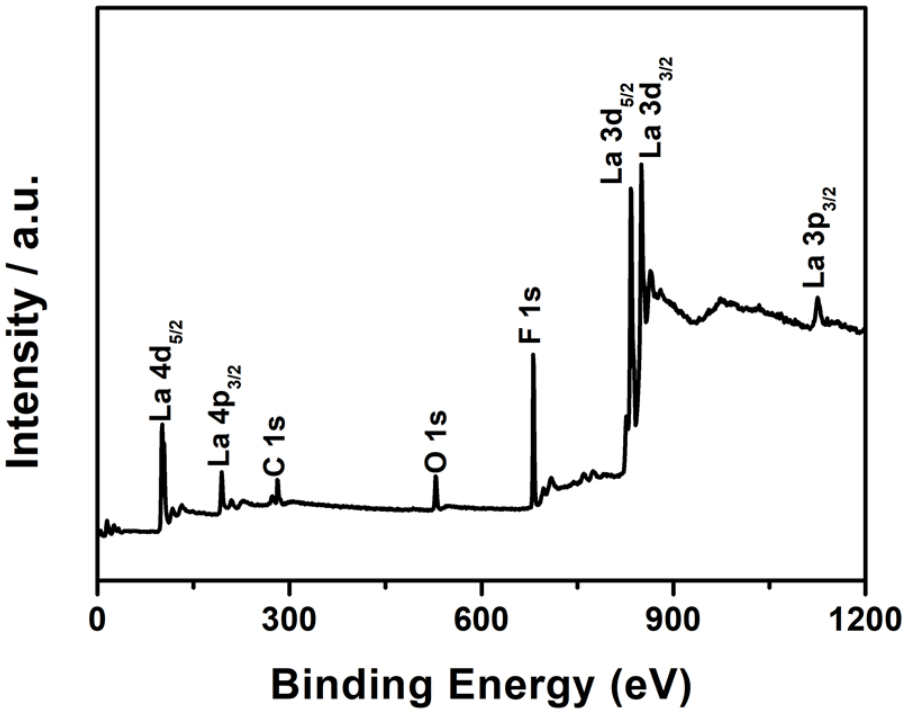

Figure S8. XPS survey spectrum of the Fv-LaF_3-2 NSs.

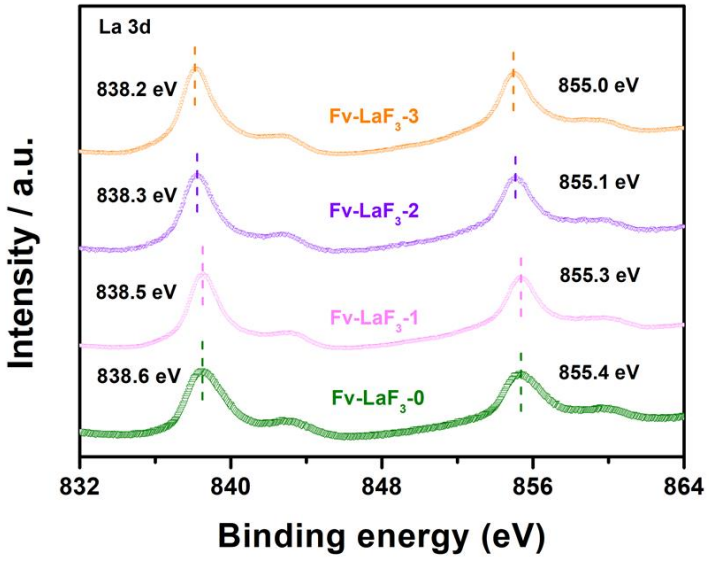

Figure S9. XPS spectra of the Fv-LaF_3-x (x=0, 1, 2, 3) NSs: La 3d.

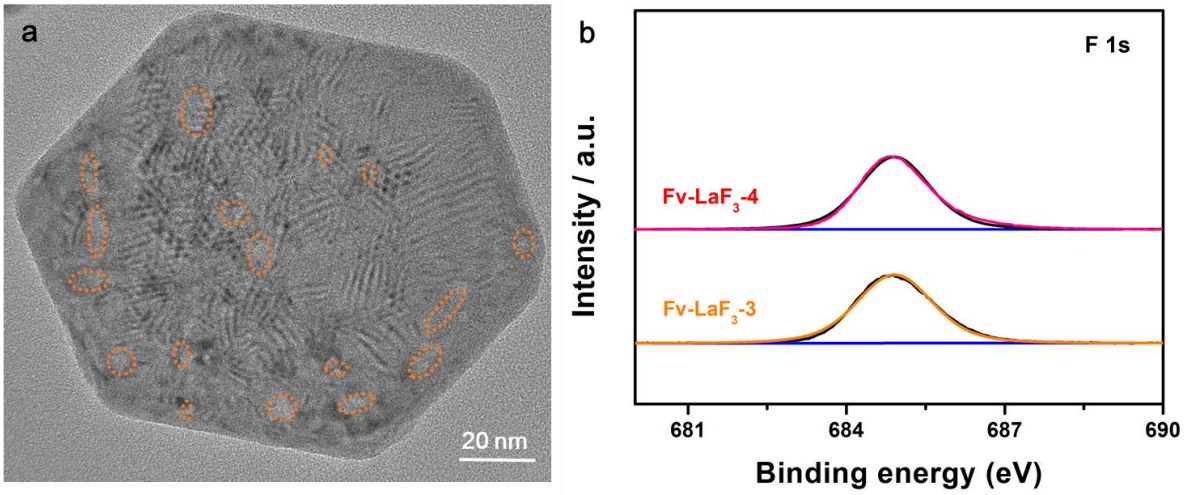

Figure S10. (a) TEM image of Fv-LaF_3-4 NSs. (b) XPS spectra of Fv-LaF_3-3 NSs and Fv-LaF_3-4 NSs: F 1s.

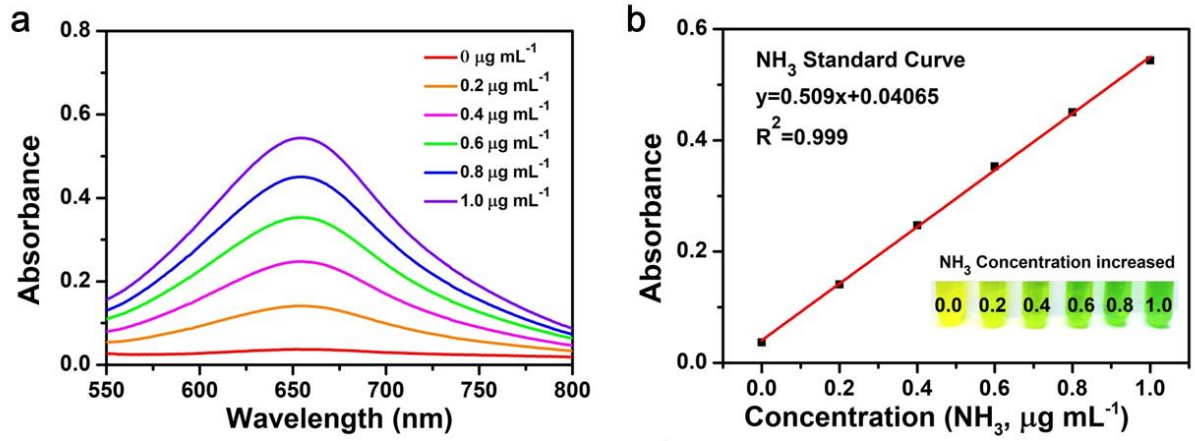

Figure S11. NH_3 quantification using indophenol blue method. (a) The UV-vis absorption spectra and (b) corresponding calibration curves for the colorimetric NH_3 assay using the indophenol blue method in 0.1 M Li_2SO_4 solution.

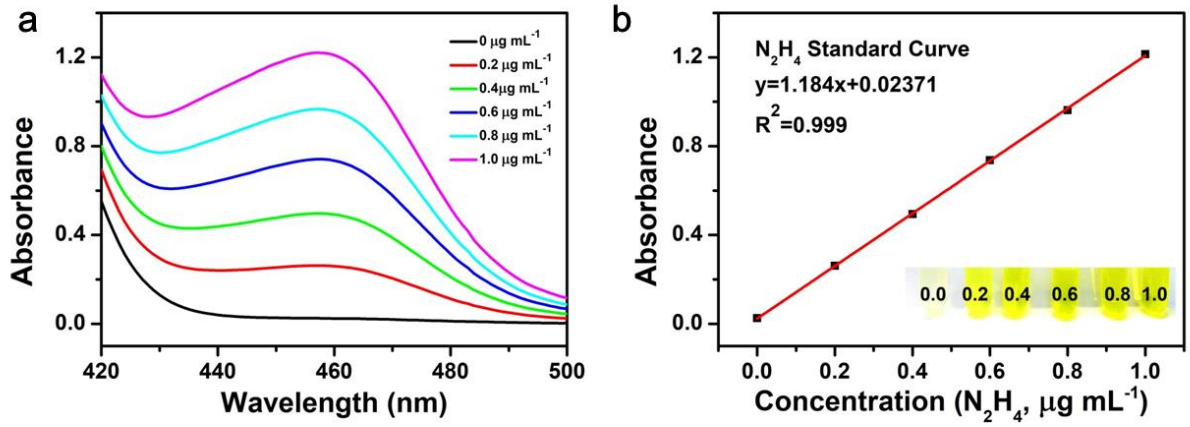

Figure S12. (a) UV-vis absorption spectra of various N_2H_4 concentration after incubated for 10 min at room temperate. (b) Calibration curve used for calculation of N_2H_4 concentrations.

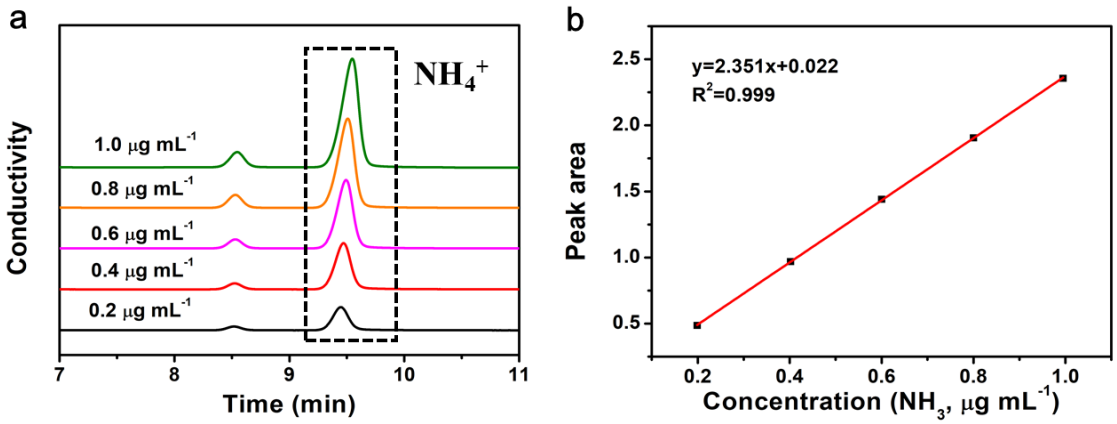

Figure S13. NH_3 quantification using IC method. (a) The IC and (b) corresponding calibration curve used for estimation of NH_4^+.

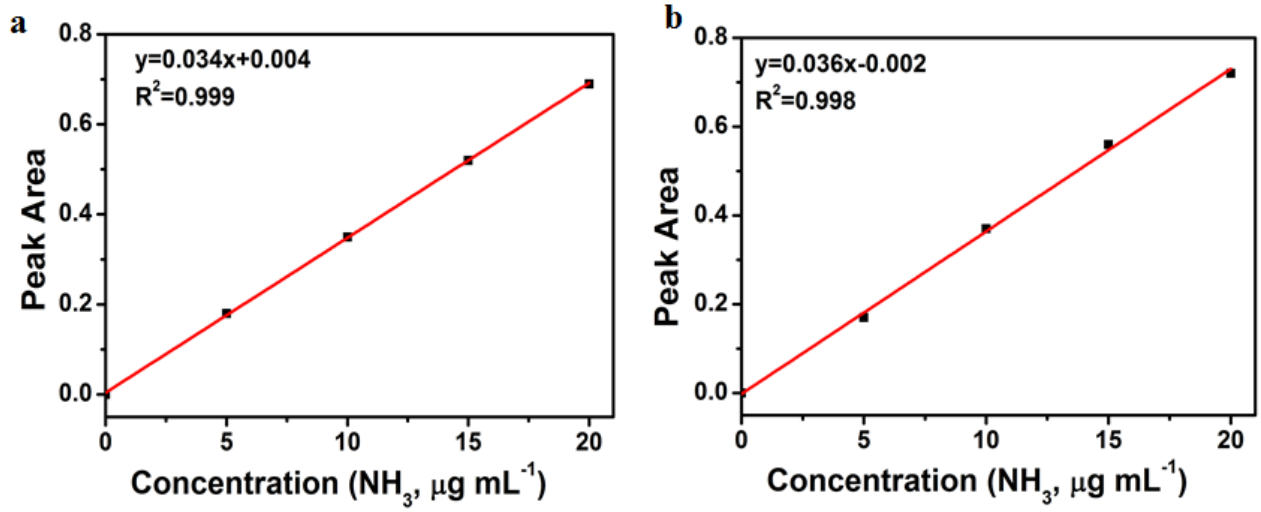

Figure S14. The calibration ^{1}H-NMR curves of produced (a) Calibration curve used for calculation of $^{14}NH_4$ concentrations. (b) Calibration curve used for calculation of $^{15}NH_4$ concentrations.

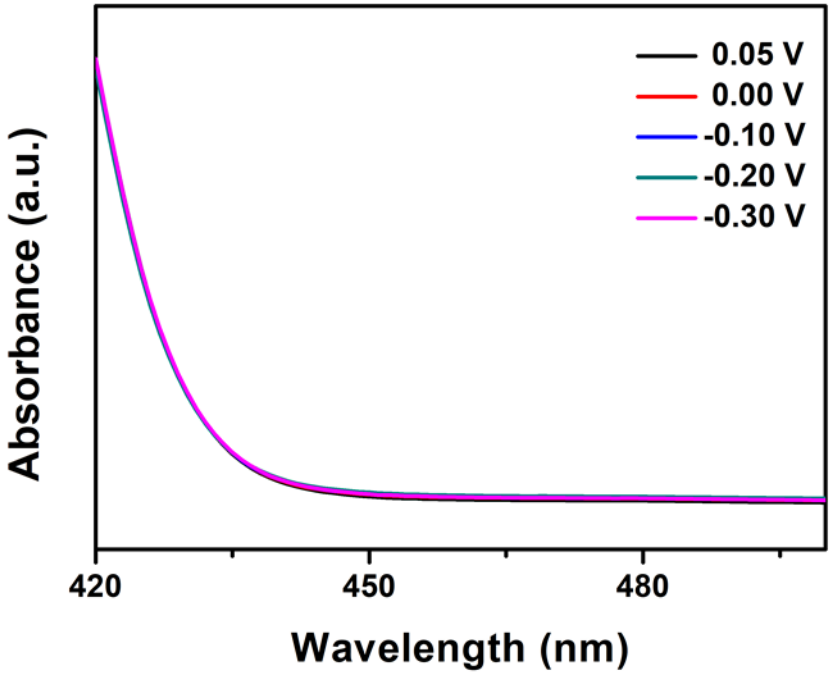

Figure S15. UV-vis absorption spectra of the electrolyte after electrolysis at different potentials.

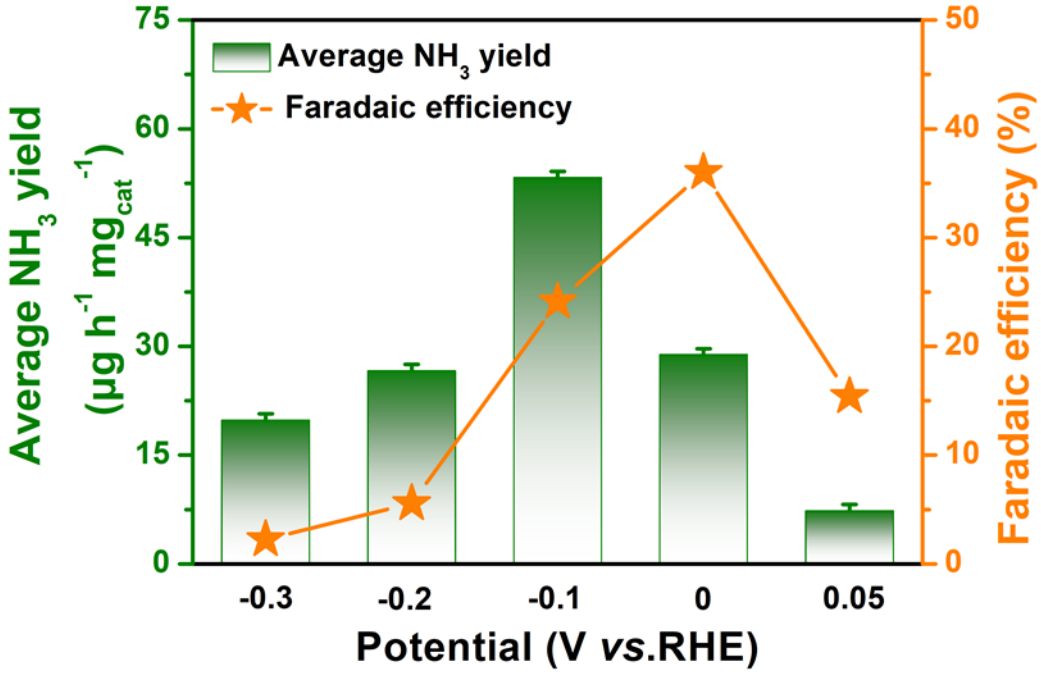

Figure S16. The FE and NH_3 yield rate of Fv-LaF_3-2 NS/CP at different potentials.

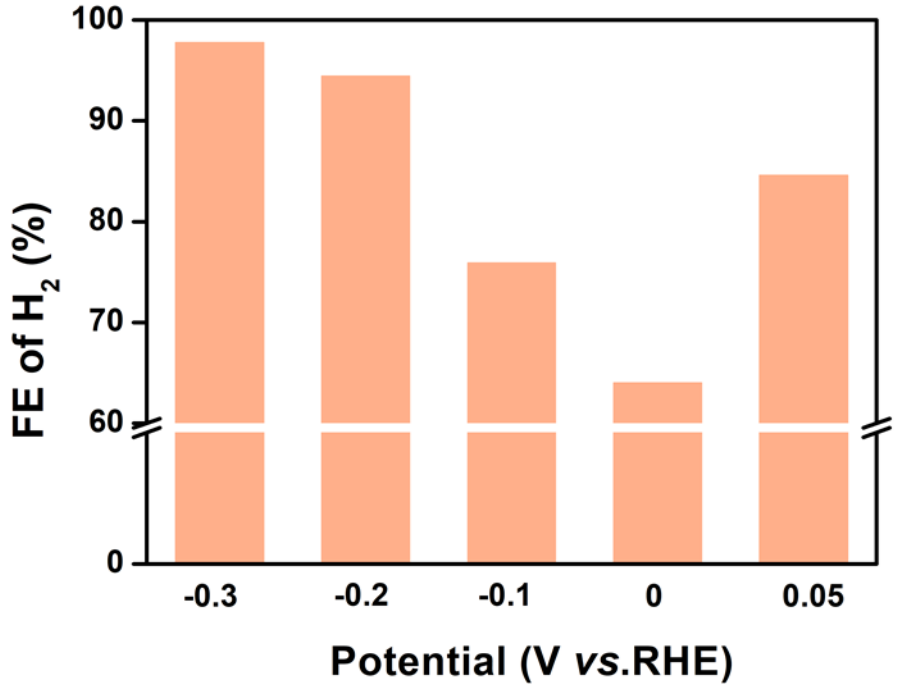

Figure S17. The FE of H_2 for Fv-LaF_3-2 NSs/CP at given potentials in 0.1 M Li_2SO_4 solution.

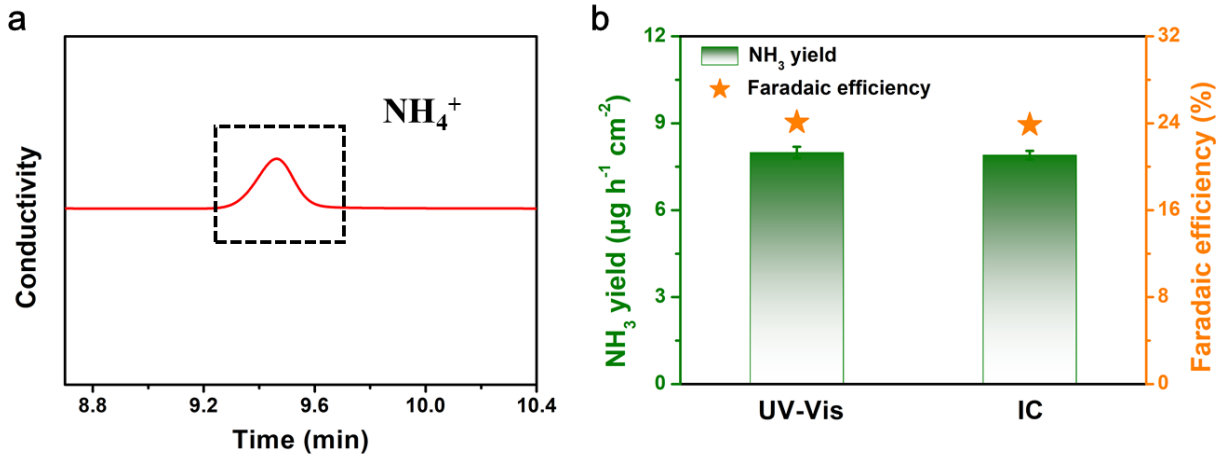

Figure S18. (a) IC result of Fv-LaF_3-2 NSs in 0.1 M Li_2SO_4 electrolyte after 1 h electrolysis under N_2 at -0.10 V *vs*. RHE. (b) Comparison chart of UV-vis absorption spectra and ion chromatography method for NH_3 yield of Fv-LaF_3-2 NSs in 0.1 M Li_2SO_4 electrolyte after 1 h electrolysis under N_2 at -0.10 V *vs*. RHE.

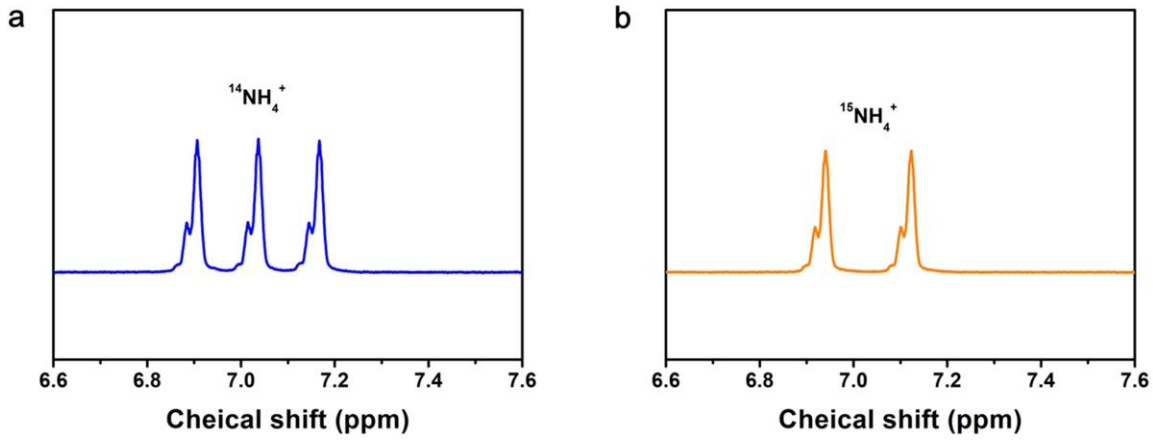

Figure S19. ^{15}N isotope labeling experiment of Fv-LaF_3-2 NSs. The ^{1}H-NMR spectrum of electrolysis in (a) $^{14}N_2$-saturated and (b) $^{15}N_2$-saturated 0.1 M Li_2SO_4 electrolyte.

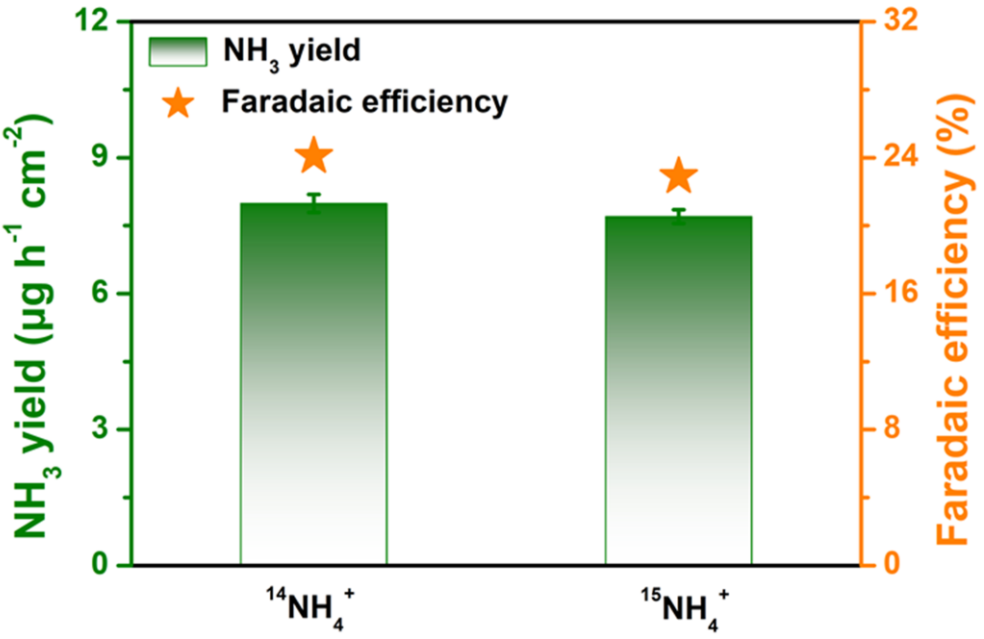

Figure S20. The NH_3 yield rate and FE of Fv-LaF_3-2 NSs at -0.10 V *vs*. RHE detected by ^{1}H NMR.

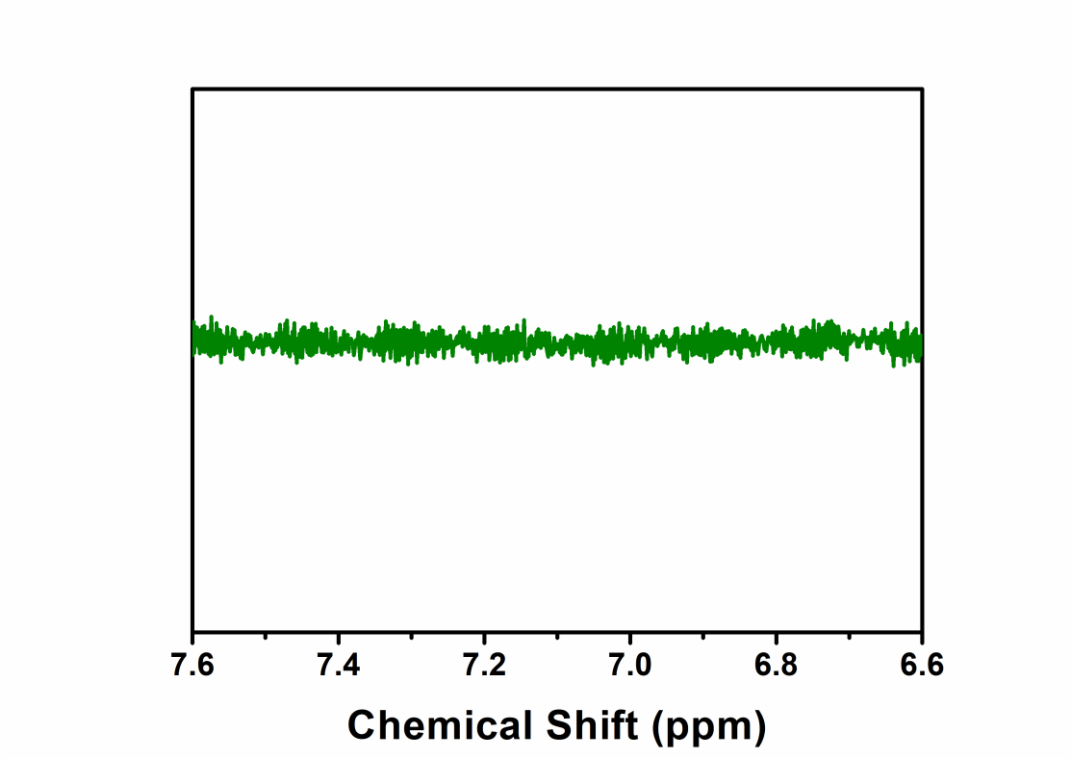

Figure S21. The ^{1}H-NMR characterization in Ar-saturated Li_2SO_4 solution.

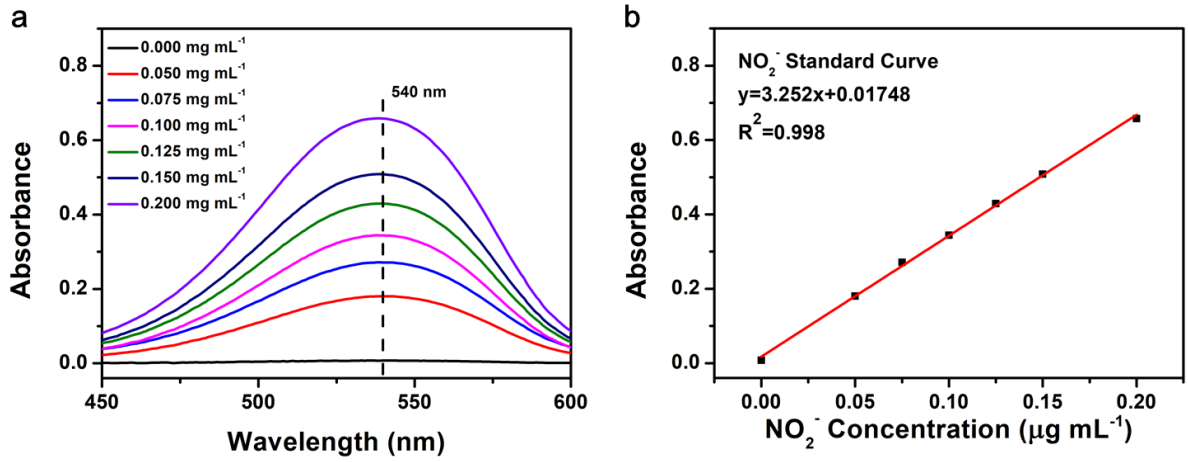

Figure S22. (a) UV-vis absorption spectra of various NO_2^- concentrations after incubated for 30 min at room temperature and (b) calibration curve used for estimation of NO_2^-.

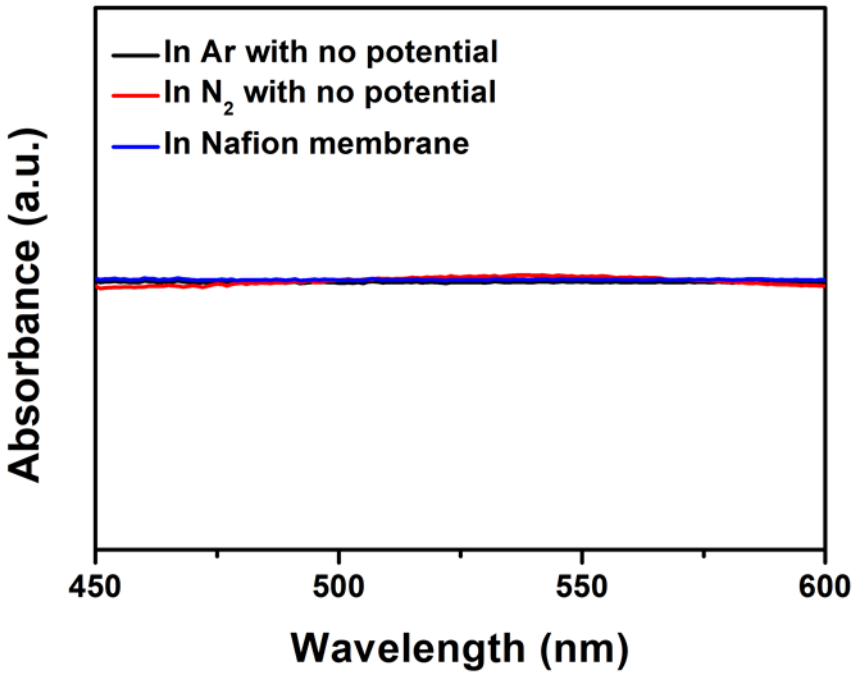

Figure S23. UV-vis absorption spectra of the electrolyte at different conditions (Black line for continuous Ar bubbling experiments with no potential applied without Fv-LaF_3-2 NSs; red line for continuous N_2 bubbling experiments with no potential applied without Fv-LaF_3-2 NSs; blue line for Nafion membrane in the cell, respectively.).

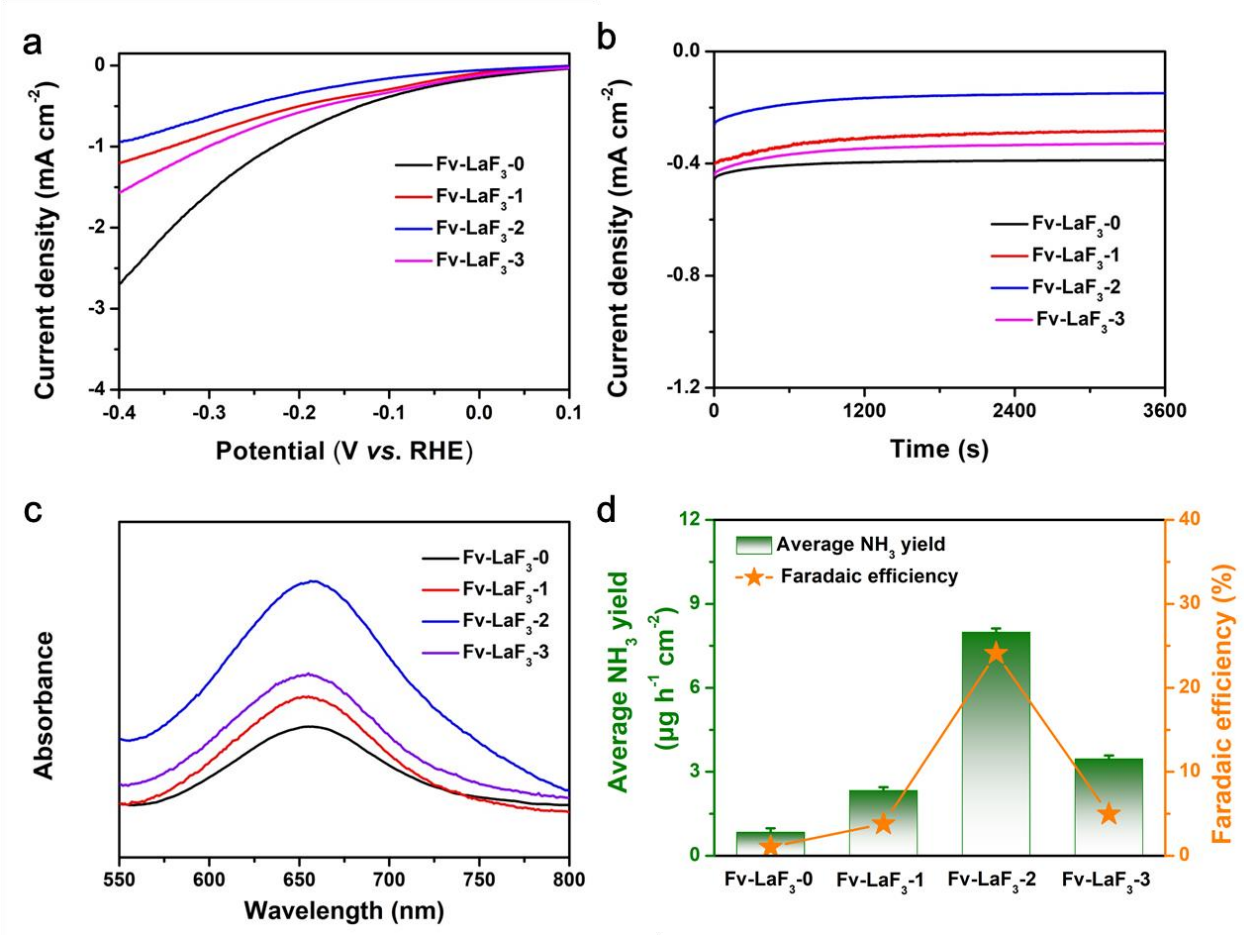

Figure S24. NRR performance of of Fv-LaF_3-x (x=0, 1, 2, 3) NSs. (a) LSV curves of Fv-LaF_3-x (x=0, 1, 2, 3) NSs in Ar- and N_2-saturated 0.1 M Li_2SO_4 with a scan rate of 10 mV s^{-1}. (b) The current-time dependent current density curves of Fv-LaF_3-x (x=0, 1, 2, 3) NSs at -0.10 V *vs*. RHE. (c) The UV-vis absorption spectra of electrolyte after electrolysis at -0.10 V *vs*. RHE. (d) The FE and NH_3 yield rate of Fv-LaF_3-x (x=0, 1, 2, 3) NSs at -0.10 V *vs*. RHE.

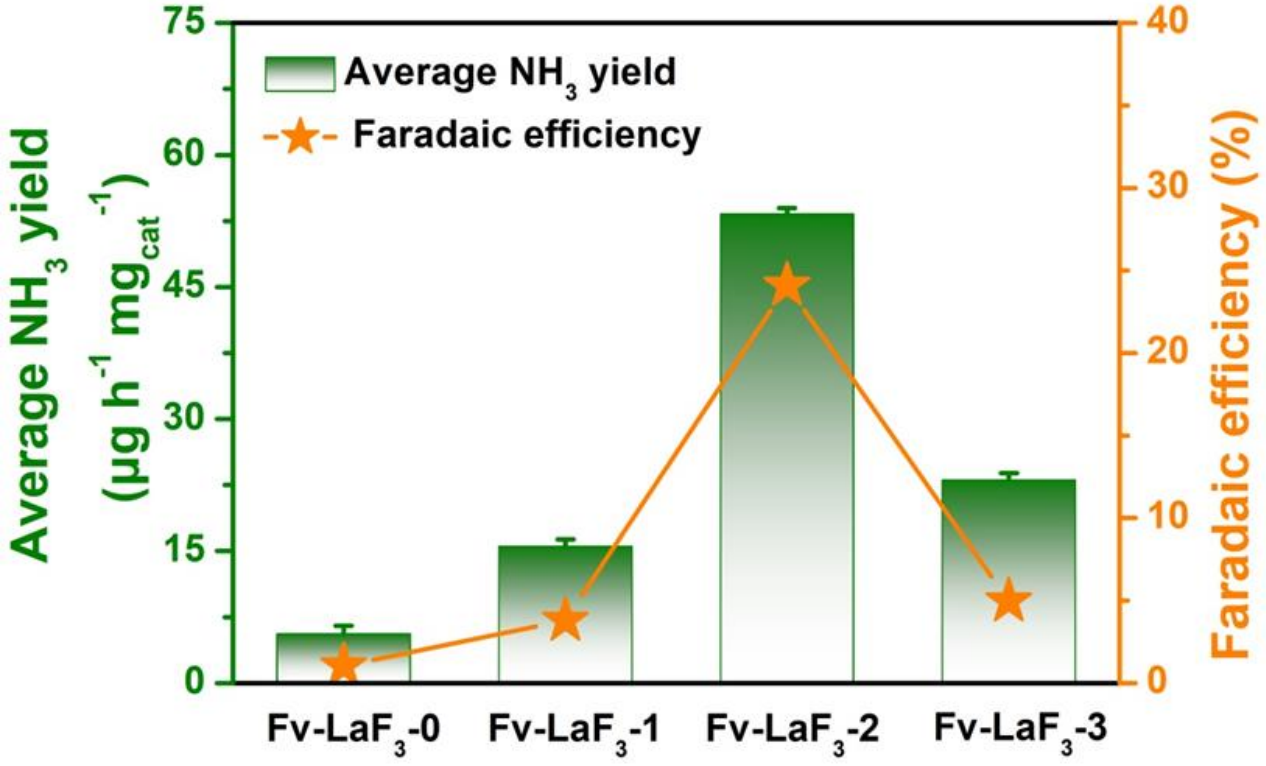

Figure S25. The FE and NH_3 yield rate of Fv-LaF_3-x (x=0, 1, 2, 3) NSs at -0.10 V *vs*. RHE.

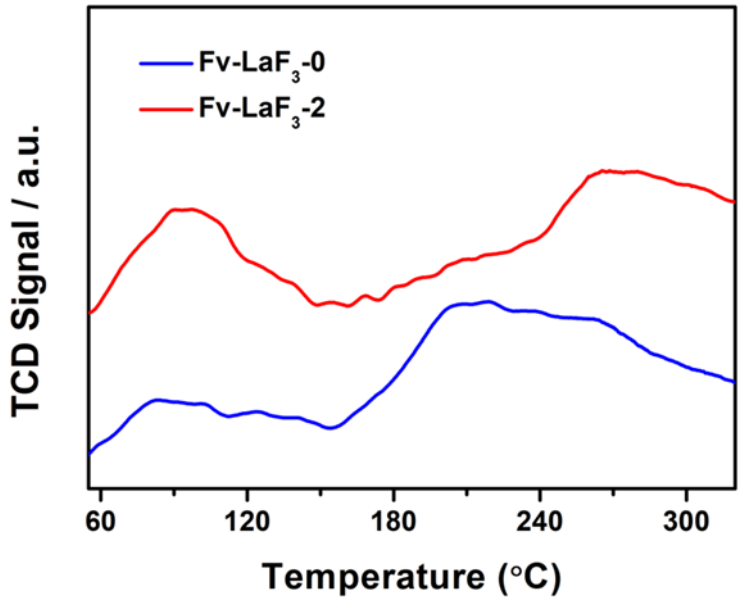

Figure S26. (a) N_2-TPD of Fv-LaF_3-0 NSs and Fv-LaF_3-2 NSs.

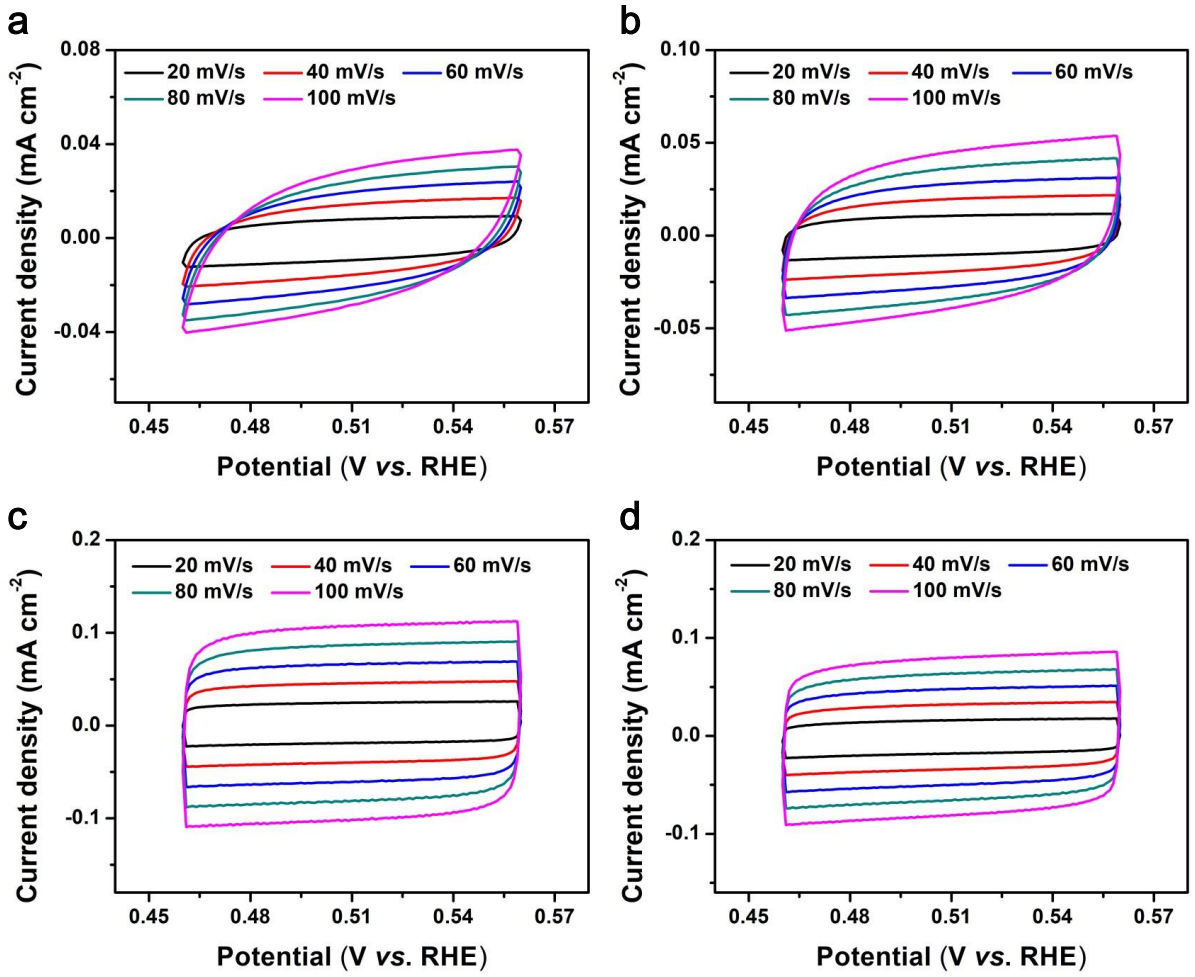

Figure S27. Cyclic voltammograms for (a) Fv-LaF_3-0 NSs, (b) Fv-LaF_3-1 NSs, (c) Fv-LaF_3-2 NSs and (d) Fv-LaF_3-3 NSs at scan rates of 20, 40, 60, 80 and 100 mV s^{-1}.

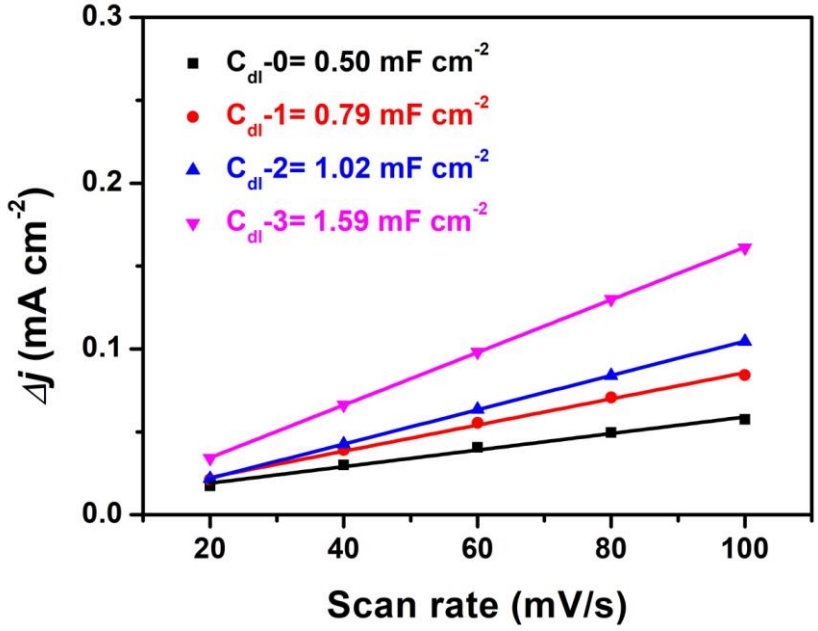

Figure S28. The capacitive currents at 0.51 V *vs*. RHE as a function of scan rate for Fv-LaF_3-x (x = 0, 1, 2, 3) NSs at scan rates of 20, 40, 60, 80 and 100 mV s^{-1}.

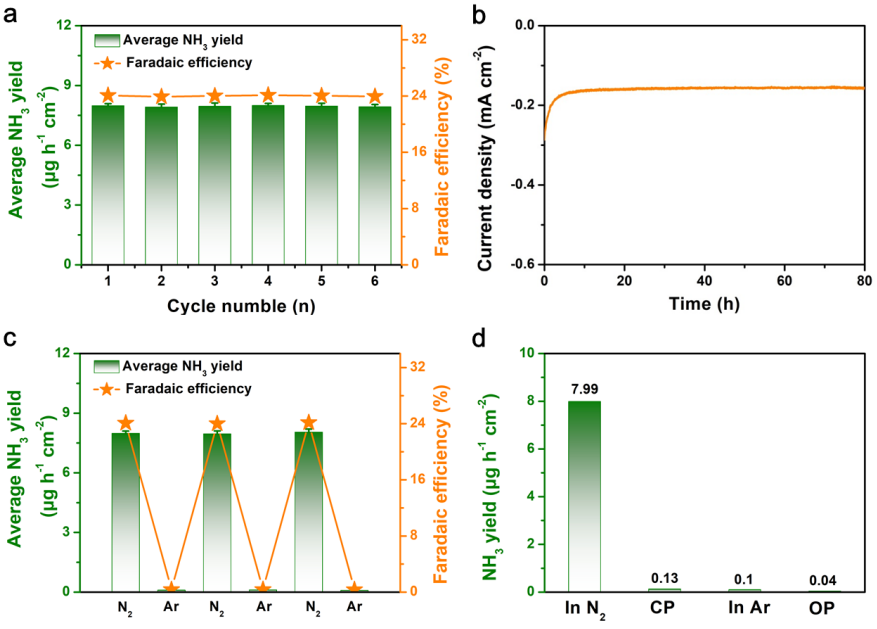

Figure S29. (a) NH_3 yields and corresponding FEs of Fv-LaF_3-2 NSs/CP at -0.10 V *vs*. RHE in N_2-saturated solutions during different cycles for 6 times. (b) The current-time curves at -0.10 V *vs*. RHE. (c) The FE and NH_3 yield rate at -0.10 V *vs*. RHE with alternating Ar-saturated and N_2-saturated electrolytes at the interval of 2 h cycles. (d) The NH_3 production at -0.10 V *vs*. RHE under different conditions.

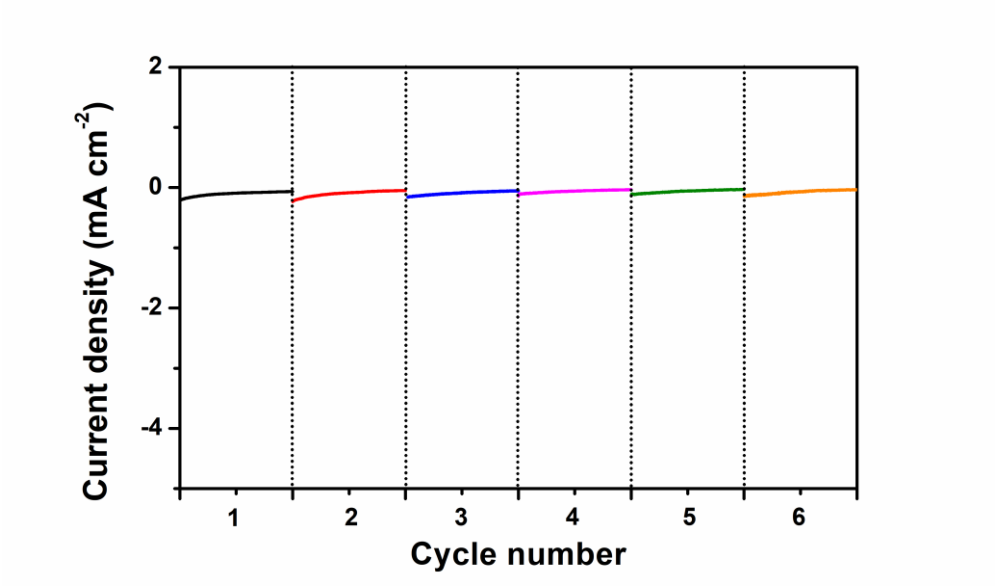

Figure S30. Time-dependent current density curves of Fv-LaF_3-2 nanosheets with 1 h for each cycle in N_2-saturated 0.1 M Li_2SO_4 solution.

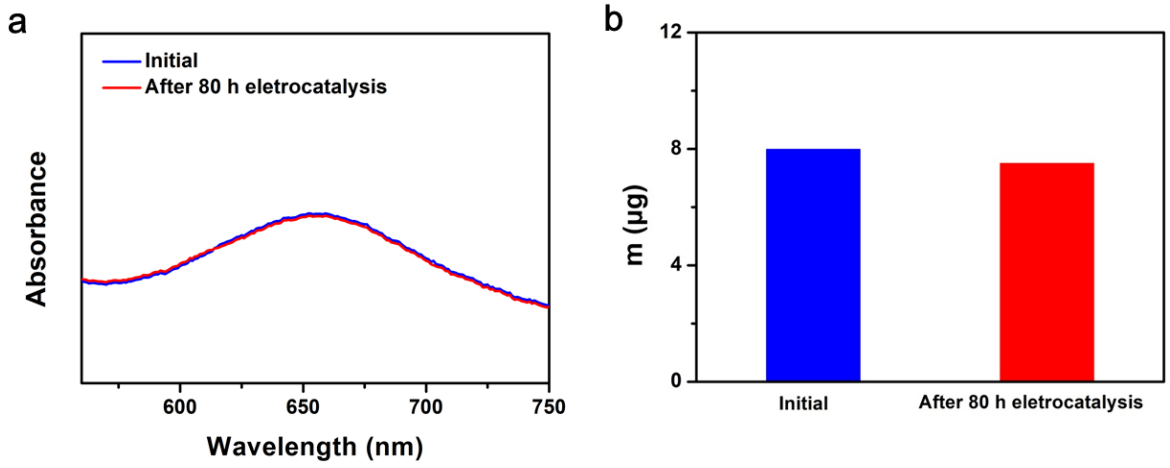

Figure S31. (a) UV-vis absorption spectra of the electrolyte stained with indophenol indicator after electrolysis at -0.10 V *vs*. RHE for 1 h over initial Fv-LaF_3-2 NSs/CP and Fv-LaF_3-2 NSs/CP subjected to 80 h. (b) Amount of NH_3 generated after 1 h electrolysis over initial Fv-LaF_3-2 NSs/CP and Fv-LaF_3-2 NSs/CP subjected to 80 h.

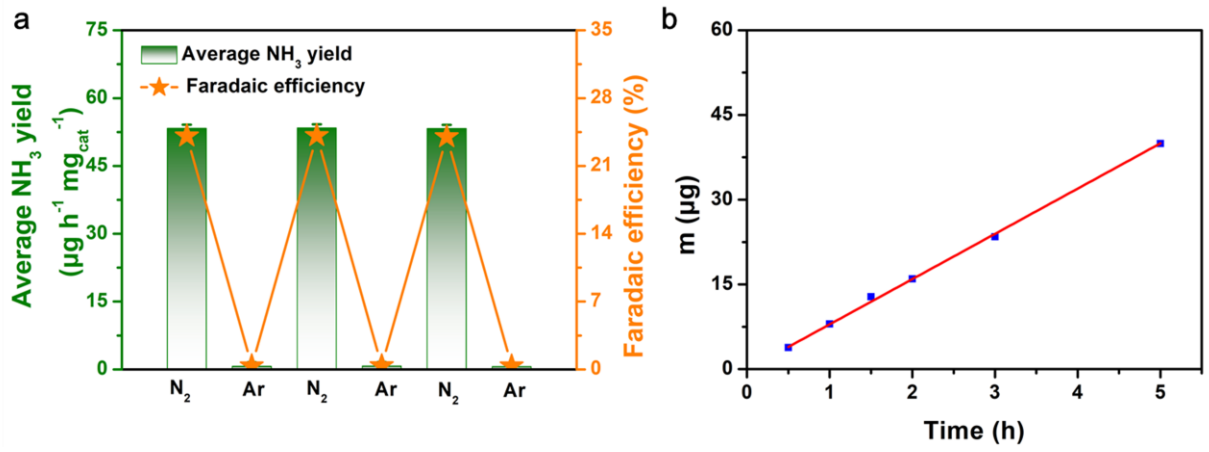

Figure S32. (a) NH_3 yields and corresponding FEs of Fv-LaF_3-2 NSs/CP with alternating 1 h cycles at -0.10 V *vs*. RHE between Ar- and N_2-saturated solutions. (b) The curve of NH_3 production *vs*. reaction time at -0.10 V *vs*. RHE.

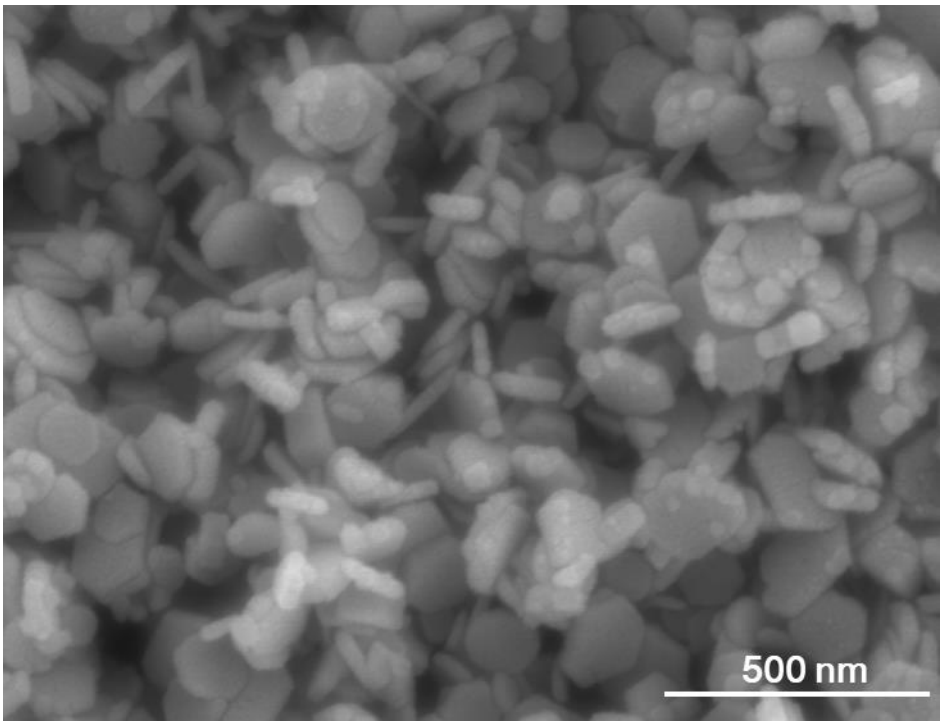

Figure S33. SEM image of Fv-LaF_3-2 NSs after stability test.

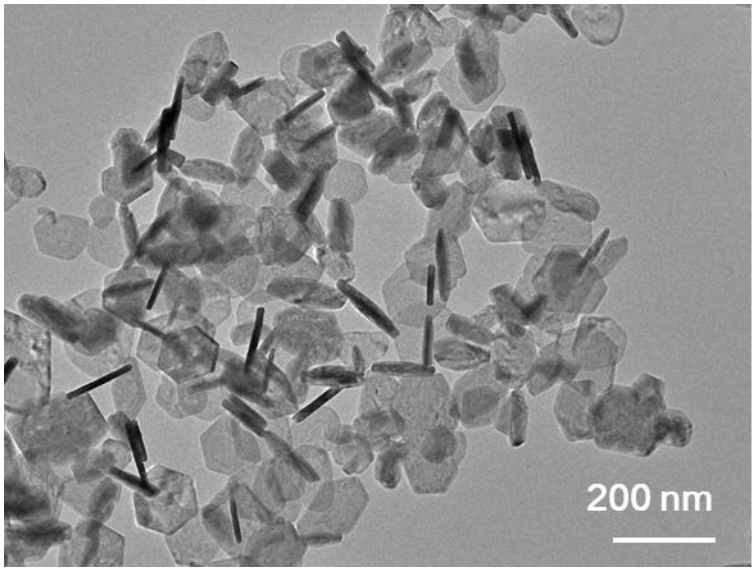

Figure S34. TEM image of Fv-LaF_3-2 NSs after stability test.

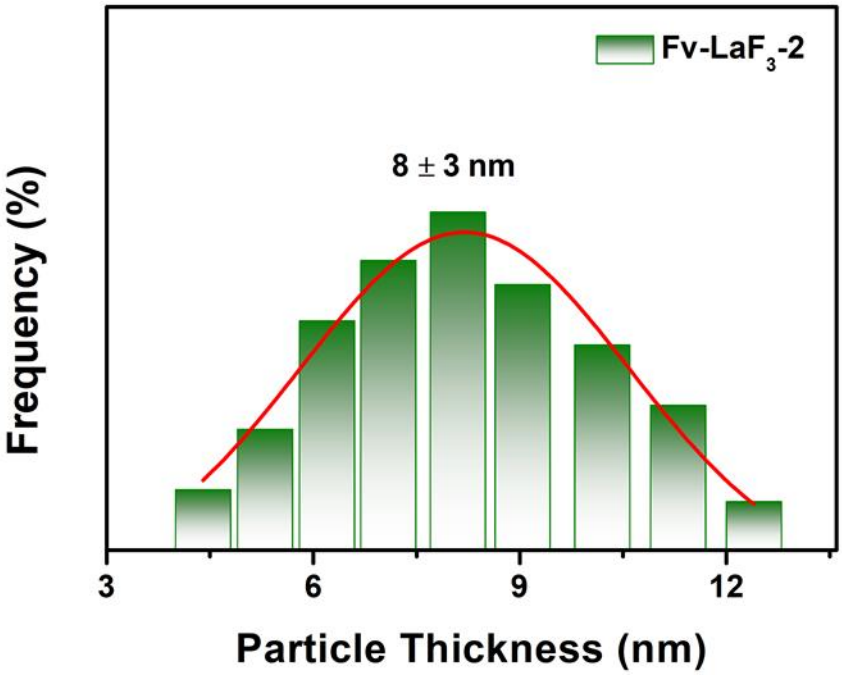

Figure S35. Particle thickness of Fv-LaF_3-2 NSs after stability test.

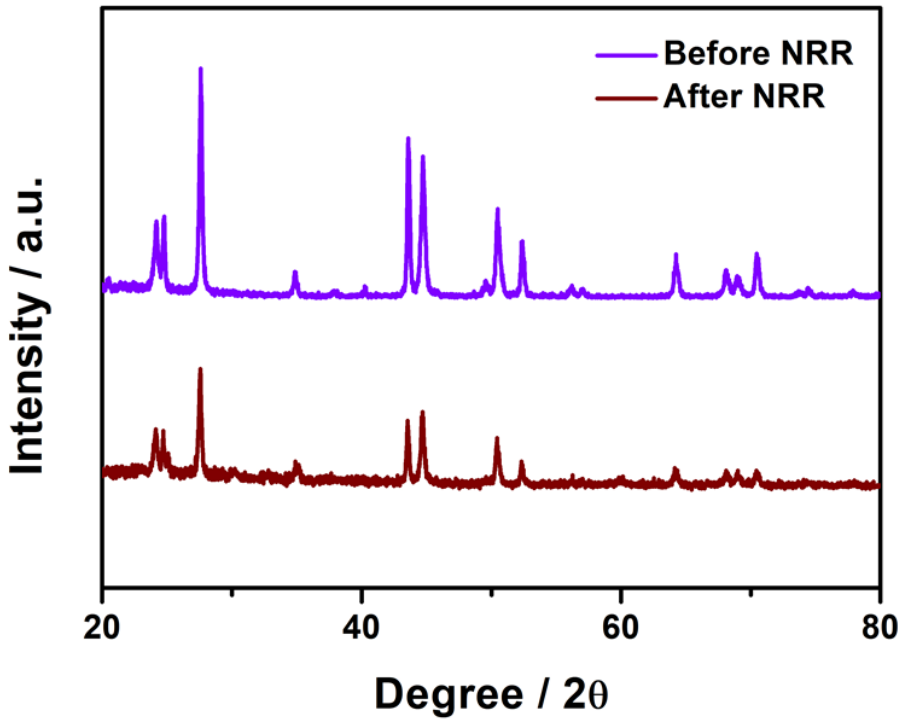

Figure S36. XRD image of Fv-LaF_3-2 NSs before and after stability test.

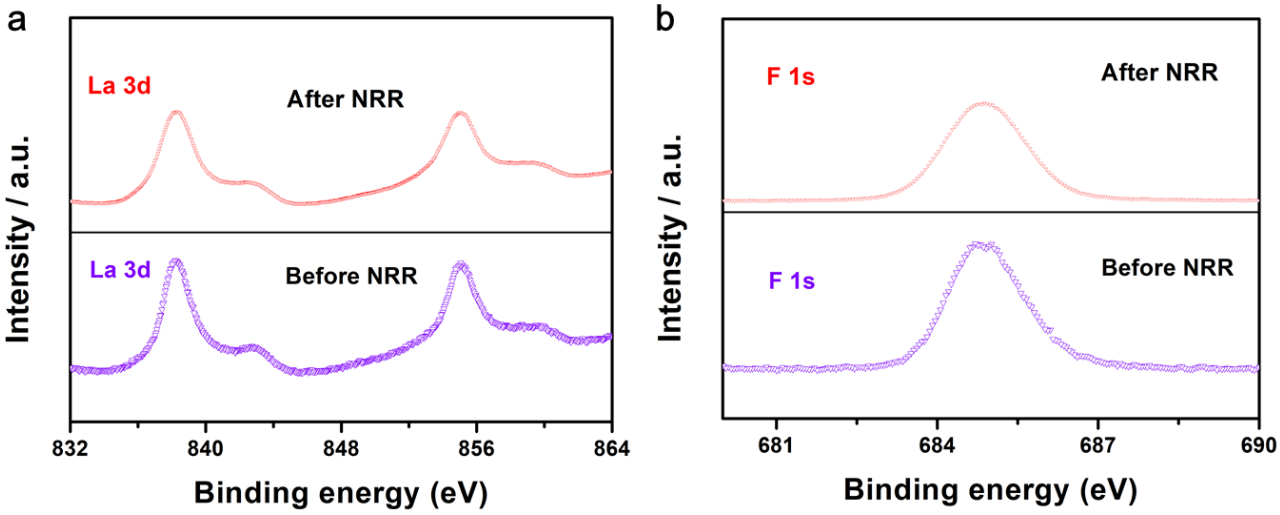

Figure S37. XPS spectras of the Fv-LaF_3-2 NSs (a) La 3d and (b) F 1s before and after stability test.

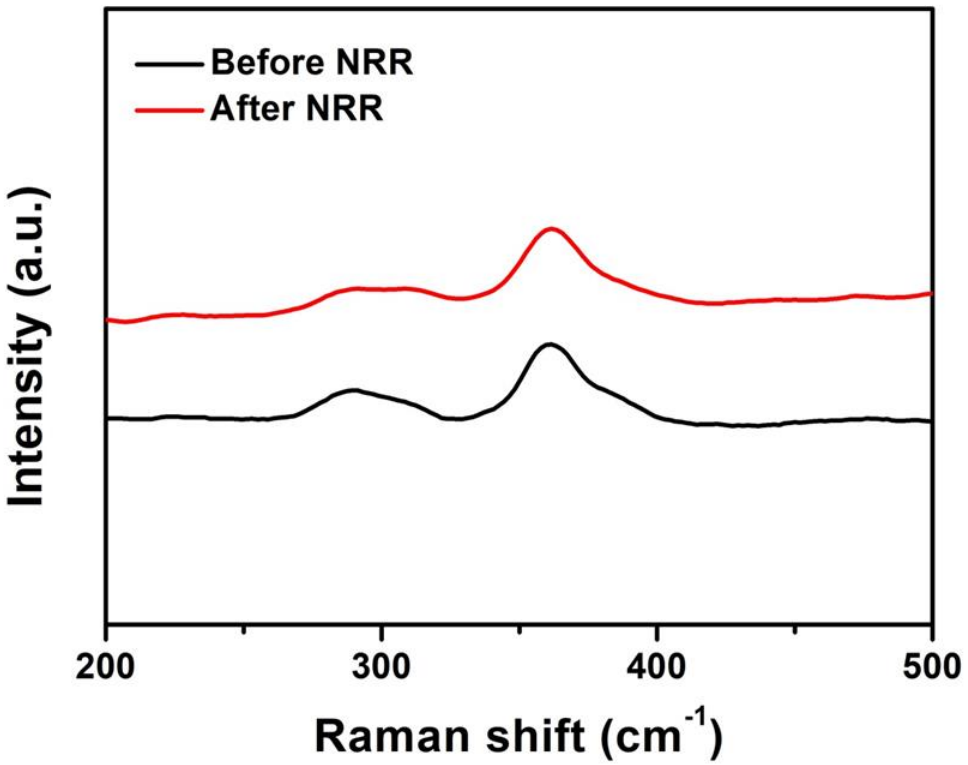

Figure S38. Raman spectra of Fv-LaF_3-2 NSs before and after stability test.

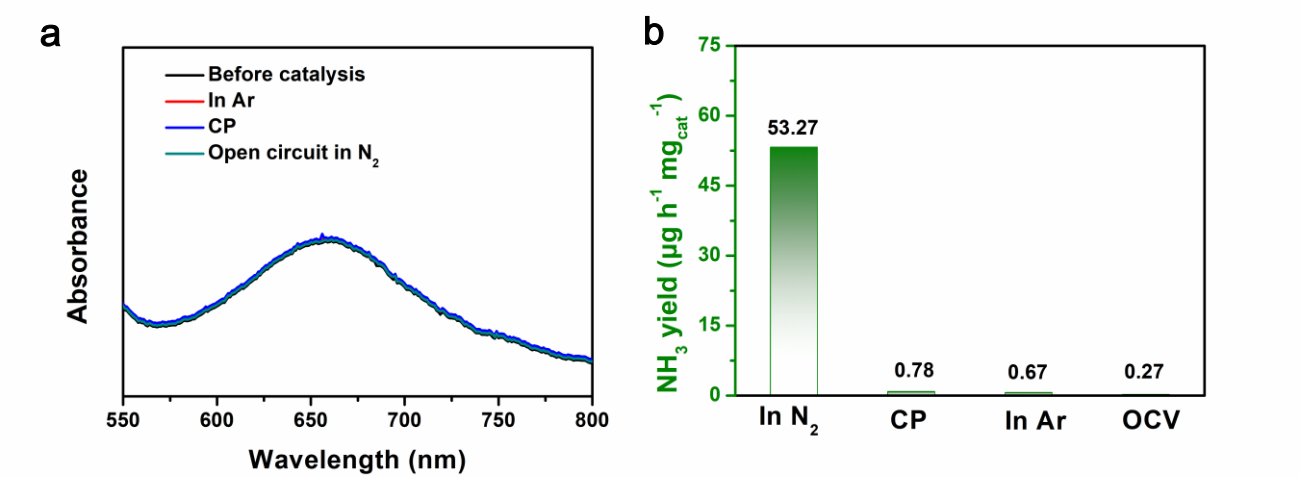

Figure S39. (a) The UV-vis absorption curves of Fv-LaF_3-2 NSs under different conditions. (b) The NH_3 yields under different conditions.

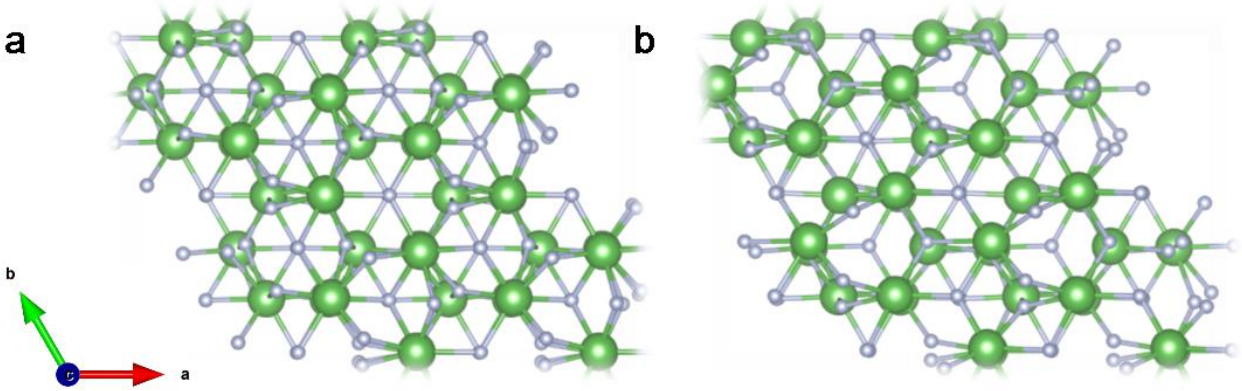

Figure S40. Optimized structure the N_2-adsorpted configuration on Fv-LaF_3-0 NSs surface (a), Fv-LaF_3-2 NSs surface (b), respectively. Gree and cyan balls represent La and F, respectively.

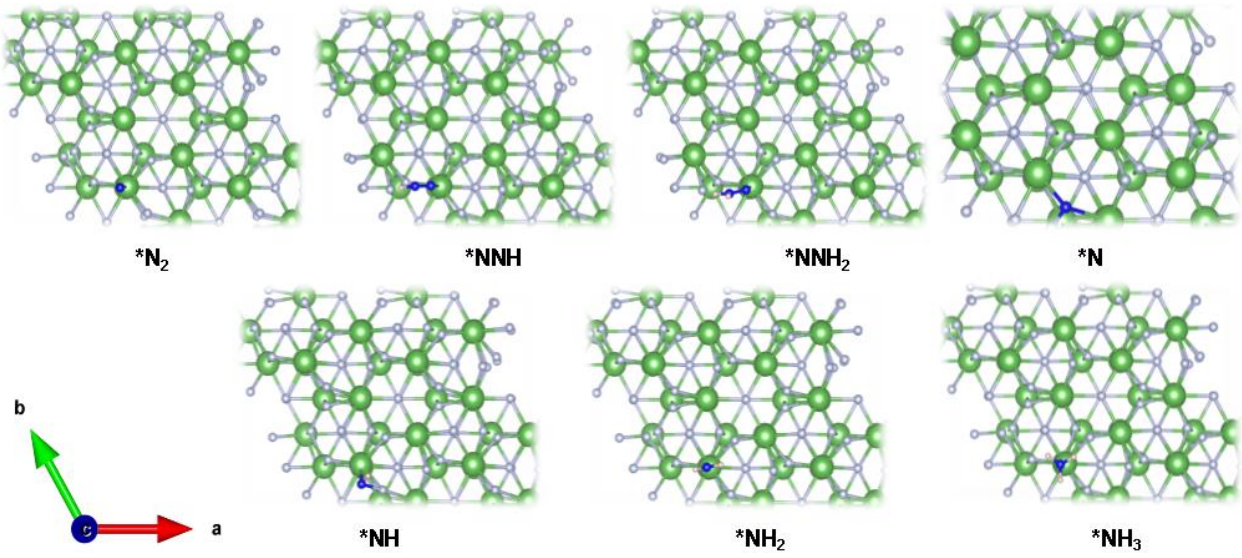

Figure S41. The optimized geometries of reaction intermediates for N_2 reduction on Fv-LaF_3-0 NSs. Gree, cyan, blue and pink balls represent La, F, N and H atoms, respectively.

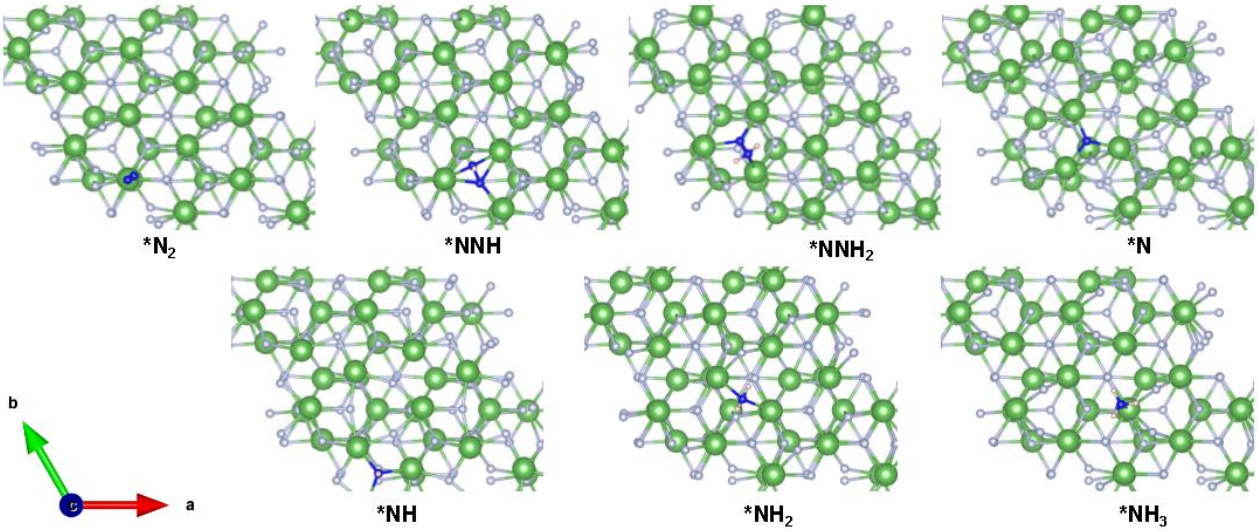

Figure S42. The optimized geometries of reaction intermediates for N_2 reduction on Fv-LaF_3-2 NSs. Gree, cyan, blue and pink balls represent La, F, N and H atoms, respectively.

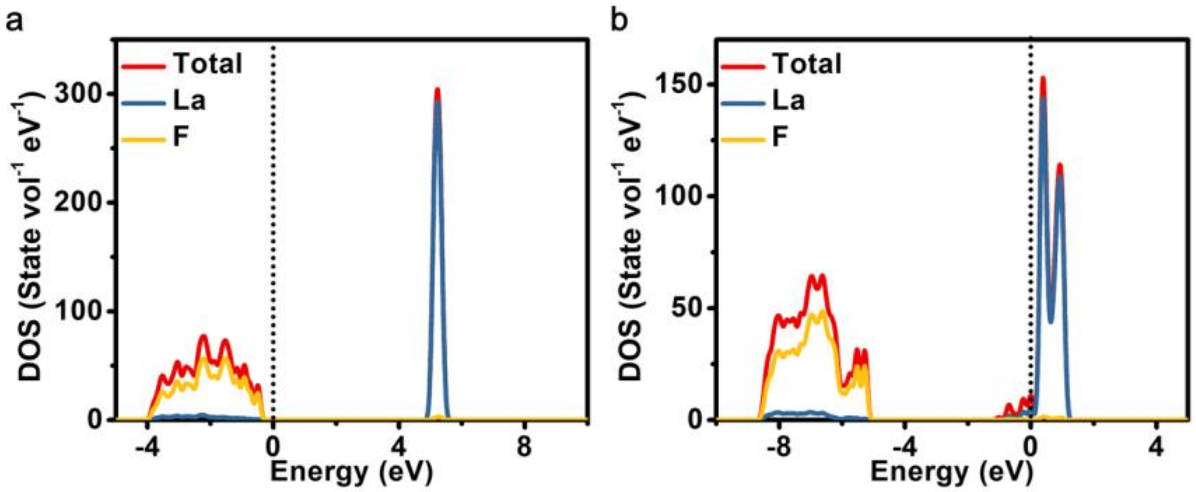

Figure S43. (a) DOS for Fv-LaF_3-0 NSs and Fv-LaF_3-2 NSs (the Fermi level is set at 0 eV).

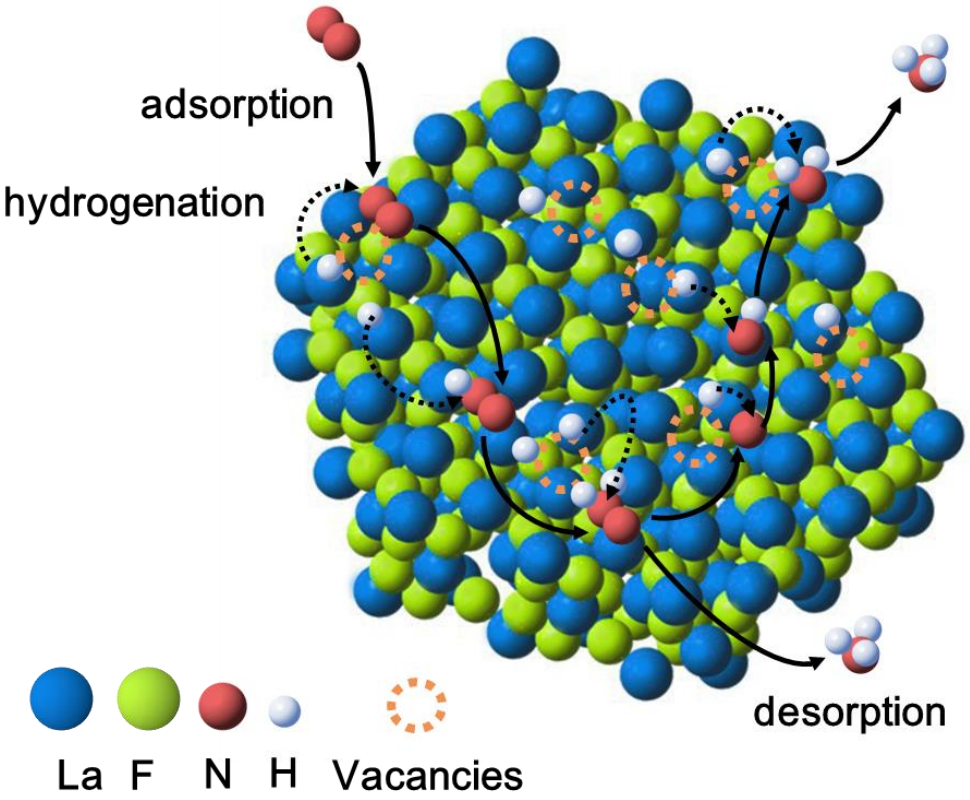

Figure S44. Concise mechanism of N_2 fixation on the surface of Fv-LaF_3-2 NSs.

Table S1. The mass ratio of fluorine and lanthanum in LaF_3 NSs with different reduction times obtained by XPS.

	Fv-LaF_3-0	Fv-LaF_3-1	Fv-LaF_3-2	Fv-LaF_3-3	Fv-LaF_3-4
La	72.99	75.32	75.95	76.25	76.31
F	27.01	24.68	24.05	23.75	23.69

Table S2. Relative Gibbs free energies (in eV) for the different states along NRR mechanism at standard conditions (298.15 K).

		N_2*	**NNH***	**NNH_2***	**N***	**NH***	**NH_2***	**NH_3***	**NH_3(g)**
	0	1	2	3	4	5	6	7	8
free	0.00	-0.09	2.01	1.49	3.29	2.62	0.67	-2.79	-2.15
defect	0.00	-0.17	-3.17	-2.61	-4.09	-4.09	-3.57	-2.76	-2.15

Table S3. Summary of the representative reports on artificially N_2 fixation.

Catalyst	Electrolyte	Potential (V *vs.* RHE)	NH_3 Yield	FE (%)	References
Fv-LaF_3-2 NSs	0.1 M Li_2SO_4	-0.10	7.99 μg cm^{-2} h^{-1} (53.27 μg mg^{-1}_{cat} h^{-1})	24.09	This work
γ-Fe_2O_3	0.1 M KOH	0	0.21 μg cm^{-2} h^{-1}	1.9	4
NiCoS/C	0.1 M Li_2SO_4	0	26.0 μg mg^{-1} h^{-1}	12.9	5
CoP	1.0 M KOH	0	2.48 μg mg^{-1}_{cat} h^{-1}	7.36	6
Fe_{SA}-N-C	0.1 M KOH	0	7.48 μg mg^{-1}_{cat} h^{-1}	56.55	7
PC/Sb/$SbPO_4$	0.1 M HCl	-0.05	3.5 μg mg^{-1}_{cat} h^{-1}	6.2	8
Mo^0/GDY	0.1 M HCl	-0.05	0.55 μg mg^{-1}_{cat} h^{-1}	7.0	9
Mo_2N@Ti	0.1 M HCl	-0.05	2.73 μg mg_{cat}^{-1} h^{-1}	28.4	10
Ti_3C_2	0.1 M KOH	-0.1	0.5 μg cm^{-2} h^{-1}	21.3	11
MoS_2	0.1 M KOH	-0.1	8.35 μg cm^{-2} h^{-1}	16.1	12
NV-W_2N_3	0.1 M KOH	-0.1	0.94 μg cm^{-2} h^{-1}	10.1	13
MoSAs-Mo_2C/NC NTs	0.1 M PBS	-0.15	5.8 μg cm^{-2} h^{-1}	8.9	14
CN/C_{500}	0.1 M HCl	-0.1	0.4 μg mg^{-1}_{cat} h^{-1}	16.8	15
Mo_3Fe_3C	0.1 M Li_2SO_4	0.05	42.2 μg mg^{-1}_{cat} h^{-1}	44.3	16

References

1. L. Zhang, L. Ding, G. Chen, X. Yang, H. Wang, *Angew. Chem. Int. Ed.,* 2018, **58**, 2612-2642.
2. X. Zhu, T. Wu, L. Ji, C. Li, T. Wang, S. Wen, S. Gao, X. Shi, Y. Luo, Q. Peng, X. Sun, *J. Mater. Chem. A*, 2019, **7**, 16117.
3. C. Yang, B. Huang, S. Bai, Y. Feng, Q. Shao, X. Huang, *Adv. Mater,*. 2020, **32**, 2001267.
4. J. Kong, A. Lim, C. Yoon, J. Jang, H. Ham, J. Han, S. Nam, D. Kim, Y. Sung, J. Choi, H. Park, *ACS Sustain. Chem. Eng.*, 2017, **5**, 10986.
5. X. Wu, Z. Wang, Y. Han, D. Zhang, M. Wang, H. Li, H. Zhao, Y. Pan, J. Lai, L. Wang, *J. Mater. Chem. A*, 2020, **8**, 543.
6. W. Guo, Z. Liang, J. Zhao, B. Zhu, K. Cai, R. Zou, Q. Xu, *Small Methods*., 2018, **2**, 1800204.
7. M. Wang, S. Liu, T. Qian, J. Liu, J. Zhou, H. Ji, J. Xiong, J. Zhong, C. Y an, *Nat. Commun.*, 2019, **10**, 341.
8. X. Liu, H. Jang, P. Li, J. Wang, Q. Qin, M. G. Kim, G. Li, J. Cho, *Angew. Chem. Int. Ed.*, 2019, **58**, 13329-13334.
9. L. Hui, Y. Xue, H. Yu, Y. Liu, Y. Fang, C. Xing, B. Huang, Y. Li, *J. Am. Chem. Soc.*, 2019, **141**,10677-10683.
10. B. Hu, M. Hu, L. Seefeldt, T. L. Liu, *ACS Energy Lett*, 2019, **4**, 1053-1054.
11. J. Xia, Z. Yang, B. Wang, P. Wu, I. Popovs, H. Li, S. Irle, S. Dai, H. Zhu, *Nano Energy.*, 2020, **72**, 104681.
12. H. Jin, L. Li, X. Liu, C. Tang, W. Xu, S. Chen, L. Song, Y. Zheng, S. Qiao, *Adv. Mater.*, 2019, **31**, 1902709.
13. Y. Liu, M. Han, Q. Xiong, S. Zhang, C. Zhao, W. Gong, G. Wang, H. Zhang, H. Zhao, *Adv. Energy Mater.*, 2019, **9**, 1803935.
14. Y. Ma, T. Yang, H. Zou, Z. Kou, L. Mao, Y. Feng, L. Shen, J. Stephen, L. Duan, X. Li, J. Wang, *Adv. Mater.* 2020, 2002177.
15. G. Peng, J. Wu, M. Wang, J. Niklas, H. Zhou, C. Liu. *Nano Lett.* 2020, **20**, 2879-2885.
16. B. Qin, Y. Li, Q. Zhang, G. Yang, H. Liang, F. Peng, *Nano Energy*.2020, **68**, 104374.